Lappeenrannan teknillinen korkeakoulu
Lappeenranta University of Technology

Juha Kaikko

PERFORMANCE PREDICTION OF GAS TURBINES BY SOLVING A SYSTEM OF NON-LINEAR EQUATIONS

Tieteellisiä julkaisuja
Research papers
68

DISCLAIMER

Portions of this document may be illegible electronic image products. Images are produced from the best available original document.

Lappeenrannan teknillinen korkeakoulu
Lappeenranta University of Technology

Juha Kaikko

PERFORMANCE PREDICTION OF GAS TURBINES BY SOLVING A SYSTEM OF NON-LINEAR EQUATIONS

Thesis for the degree of Doctor of Technology to be presented with due permission for public examination and criticism in the Auditorium in the Students' Union Building at Lappeenranta University of Technology, Lappeenranta, Finland on the 6th of March, 1998, at noon.

Tieteellisiä julkaisuja
Research papers
68

ISBN 951-764-142-7
ISSN 0356-8210

Lappeenrannan teknillinen korkeakoulu
Monistamo 1998

ABSTRACT

Lappeenranta University of Technology
Research papers 68

Juha Kaikko
Performance Prediction of Gas Turbines by Solving a System of Non-Linear Equations
Lappeenranta, 1998

91 pages, 27 figures, 10 tables

ISBN 951-764-142-7, ISSN 0356-8210 UDK 621.438 : 519.6

Key words: gas turbine, performance, design, off-design, part-load, mathematical models

This study presents a novel method for implementing the performance prediction of gas turbines from the component models. It is based on solving the non-linear set of equations that corresponds to the process equations, and the mass and energy balances for the engine. General models have been presented for determining the steady state operation of single components. Single and multiple shaft arrangements have been examined with consideration also being given to heat regeneration and intercooling. Emphasis has been placed upon axial gas turbines of an industrial scale. Applying the models requires no information of the structural dimensions of the gas turbines.

On comparison with the commonly applied component matching procedures, this method incorporates several advantages. The application of the models for providing results is facilitated as less attention needs to be paid to calculation sequences and routines. Solving the set of equations is based on zeroing co-ordinate functions that are directly derived from the modelling equations. Therefore, controlling the accuracy of the results is easy. This method gives more freedom for the selection of the modelling parameters since, unlike for the matching procedures, exchanging these criteria does not itself affect the algorithms. Implicit relationships between the variables are of no significance, thus increasing the freedom for the modelling equations as well.

The mathematical models developed in this thesis will provide facilities to optimise the operation of any major gas turbine configuration with respect to the desired process parameters. The computational methods used in this study may also be adapted to any other modelling problems arising in industry.

ACKNOWLEDGEMENTS

This work has been carried out in the Section of Thermodynamics and Environmental Engineering, in the Department of Energy Technology of Lappeenranta University of Technology.

I wish to express my sincere thanks to Professor Sarkomaa, Head of the Department and my supervisor. His enthusiasm and encouragement about this study was not only the impulse, but often also the necessary thrust for me throughout the work.

I am also deeply grateful to Associate Professor Jaakko Larjola, whose advice has helped me to see the important things and the right contexts. For a young researcher, this kind of knowledge that is based on many years of experience in gas turbine technology is priceless.

Special thanks are due to the pre-examiners, Professor David Gordon Wilson from Massachusetts Institute of Technology and Professor Markku Lukka from Lappeenranta University of Technology, for their valuable corrections and comments. I also wish to thank Dr. Jari Backman for his wise criticism during the reviewing of the manuscript.

I am obliged to Mr. Graeme Stewart, B.Eng. for revising my English manuscript. The financial support of Lappeenranta University of Technology is also gratefully acknowledged.

To my colleagues in the Department, as well as to my friends, I would like to express my thanks for their encouragement during this study. The contribution of Associate Professor Heikki Kälviäinen and Mr. Jyrki Alamäki, M.Sc. has been especially important.

Most of all, I am indebted to my parents, Liisa and Aulis, as well as to my brother, Lasse. They have supported me during the years in a way that is beyond comprehension.

Lappeenranta, February 1998.

Juha Kaikko

CONTENTS

NOMENCLATURE

A	area, m^2
c	absolute velocity of fluid, m/s
c_p	specific heat capacity at constant pressure, J/(kg K)
c_0, c_1, c_2, c_3	coefficients for polynomials
CHP	combined heat and power production
d	diameter, m
$\mathbf{e}_j$	j:th unit vector
f	summary term
f_i	i:th co-ordinate function
$f_1, \ldots, f_{12}$	subroutines
$\mathbf{F}$	function vector
g	gravitational acceleration, m/s^2
g	function
h	specific enthalpy, kJ/kg
h	step size, -
ICAD	intercooled aeroderivative gas turbine
j_H	Colburn factor, -
k	isentropic exponent, -
k	overall heat transfer coefficient, $W/(m^2K)$
k	relative pressure loss, -
l	characteristic length, m
L	specific amount of air, -
LHV	lower heating value
m	mass, kg
M	molecular mass, kg/mol
M	number of stages in turbine
M	torque, Nm
M_1, M_2	local minima
n	polytropic exponent, -
n	number of dimensions
N	rotational speed, 1/s
Nu	Nusselt number, -
p	pressure, Pa
ppmv	parts per million (volumetric)
P	power, W
P_{spec}	specific power, J/kg
Pr	Prandtl number, -
q	specific heat, J/kg
q_i	lower heating value, J/kg
q_m	mass flow, kg/s
Q	heat, J
Q_m	molecular heating value, J/mol
r	reaction degree, -
R	specific gas constant, J/(kg K)
Re	Reynolds number, -
R_u	universal gas constant, J/(mol K)
s	specific entropy, J/(kg K)

St	Stanton number, -
T	temperature, K
u	circumferential velocity of fluid, m/s
u	specific internal energy, J/kg
U	internal energy, J
v	specific volume, m^3/kg
V	volume, m^3
w	velocity of fluid, m/s
w	specific work, J/kg
W	work, J
x	mole fraction, -
x	variable vector
x,y	variables
y	mass fraction, -
Y	surge margin, -
z	height, m
z	ratio of bearing losses, -

α	heat transfer coefficient, $W/(m^2 K)$
α	coefficient, -
β	characteristic blade setting angle, -
β	coefficient, -
ε	effectiveness, -
η	efficiency, -
λ	coefficient, -
λ	thermal conductivity, W/(m K)
μ	intake ratio, -
μ	dynamic viscosity, Ns/ m^2
ν	blade speed ratio, -
π	pressure ratio, -
Π	term for pressure ratio, -
ρ	density, kg/m^3
Φ	term for rotational speed, -
Φ	heat rate, W
ω	angular velocity, rad/s

Superscripts

(k)	number of successive iteration sequence
*	solution for the set of equations

Subscripts

0,...,9	cycle operation points
0	design state
a	air
a	area
amb	ambient
c	compressor
cc	combustion chamber
cg	combustion gases
co	cooling air
cr	critical
e	net
fu	fuel
gen	generator
gear	gearbox
h	hydraulic
i,j	sequence numbers
ln	logarithmic
loss	bearing loss
m	mean
mat	material
max	maximum
mech	mechanical
M	mixing
n	axial
p	polytropic
q	heat transfer
ref	reference state
rel	relative to design value
s	isentropic
s	surge
s	stoichiometric
sg	stoichiometric combustion gases
t	total state
t	turbine
t	theoretical
th	thermal
w	work
α	inlet state

1 INTRODUCTION

As long as there has been activities in gas turbine technology - from the very beginning of the 20th century - there has been a need for evaluating performance values of an actual gas turbine engine. Earlier, the methodology for determining the values has been restricted not only by the vague knowledge of, especially, compressible flow, but also the calculus itself. While there has been an immense increase in the theoretical ability to model a gas turbine process, the application for exploiting these theorems still heavily relies on the spirit of a slide rule age. That is, complex routines are characterised by consecutive matching procedures for determining the values, by trial and error. Yet, this task could be accomplished by joining the theoretical elements as a non-linear set of equations, thus providing us with all information needed without having to perform numerous configuration-based iteration routines. This alternative approach is to be demonstrated in this thesis.

A gas turbine is a sophisticated thermal power engine consisting, even in its simplest form, of a compressor, combustion chamber, turbine and a variety of auxiliary devices. While physical properties determine the behaviour of these components, interaction of the components dictates the overall performance of the gas turbine. The elementary evaluation of the gas turbine performance can be conducted at design state conditions. Due to fluctuations of ambient temperature or load, for instance, the operational state rarely complies with these conditions. Therefore, it is necessary to predict the performance of a gas turbine outside design state too, thus forming a foundation for thermal, economic and condition monitoring aspects in gas turbine technology.

This decade was faced with a boom of modelling gas turbine steady state performance. As a result, a variety of methodologies and implementations for predicting the performance of gas turbine cycles have been presented by Ismail et al. [1991], Kim et al. [1994] and Korakianitis et al. [1994a], as well as commercial software packages for performing the analysis, for example GateCycle™. A study utilising this software has been reported by Johnson [1992], for instance. Further considerations on the gas turbine cycle matching process itself have been presented by Wang [1991] and Zhu et al. [1992].

A common denominator for all these concerns is their modular and iterative nature. The component modules are constructed with analytical balance and process equations, and/or with performance characteristics, the matching calculations for these modules being based on an iterative solution process.

A study by Seyedan et al. [1995] presents a simulation procedure for predicting the performance of combined cycle power plants, using given performance characteristics of its main components. The interlinking of the flow diagrams is eventually reduced to the solution of a small set of non-linear equations.

The motivation for this thesis is to prove the feasibility of using multi-dimensional root finding methods, even for common complex gas turbine models. These models are constructed using basic mass and energy balances and process equations, with some of the information being in the form of maps for assessing the behaviour of the prime characteristics (pressure ratio, mass flow and efficiency, for instance) outside design conditions. Whilst the modelling itself is based on common practice, the methodology for determining the operational state from this starting point is new.

The physical phenomena in the gas turbine are assumed not to have any time-dependent variables, so the analysis is based on steady state conditions where all the reactions have reached the equilibrium. Properties vary only with the axial direction of the flow, the model being in this sense one-dimensional. The emphasis in this study has been placed on axial gas turbines of an industrial scale, with general validity being of primary interest.

2 THE GAS TURBINE ENGINE

Gas turbines are thermal power engines having a flow of gas compressed and heated such that during the expansion more work is generated than necessary to maintain the process. Unlike with reciprocating engines, for instance, compression, heating and expansion are continuous and they occur simultaneously.

2.1 General

Most gas turbines are based on the open Brayton cycle with internal combustion. The cycle chart is usually described as a *T,s*-chart or *h,s*-chart, as plotted in Fig. 1. In the basic cycle, Fig. 1.a, air from the ambient atmosphere is compressed to a higher pressure and temperature by the compressor. In the combustion chamber, air is heated further by burning an appropriate amount of fuel in the air flow. Combustion gases expand in the turbine either to near atmospheric pressure (engines producing mechanical energy) or to a pressure required by the jet nozzle (jet engines). In both cases, the gases are discharged into the atmosphere.

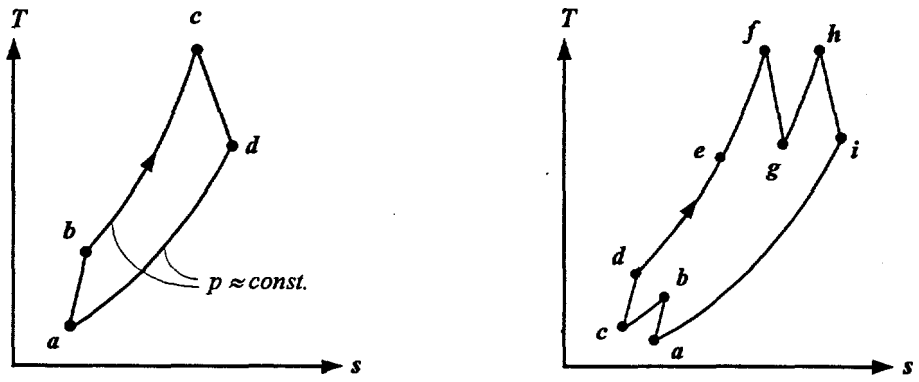

(a) *(b)*

Figure 1. *T,s*-charts of the open Brayton cycles. *a)* a basic cycle: **a→b** compression of air, **b→c** burning of fuel, **c→d** expansion of combustion gases *b)* a cycle with intercooling, heat regeneration and reheat: **a→b** 1st compression, **b→c** intercooling, **c→d** 2nd compression, **d→e** heat regeneration, **e→f** 1st combustion, **f→g** 1st expansion, **g→h** 2nd combustion, **h→i** 2nd expansion

In a closed cycle, the working fluid, hydrogen mixed with xenon for instance, is cooled after the turbine and taken to the compressor. Instead of combustion chambers, the heat addition to the cycle is obtained with a heat exchanger, the heat source being, for example, nuclear reactions.

Intercooling can be applied between compressor stages to reduce compression work, hence increasing power of the gas turbine and, to a lesser extent, the efficiency as well. During operation with moderate pressure ratios or, by using intercooling, the efficiency can be drastically increased by transferring heat from the turbine exhaust gas to the compressor discharge air flow (regeneration). This reduces the fuel amount required to heat up the air. However, pressure losses generated by the heat exchanger slightly reduce the power of the gas turbine. Sequential combustion (reheat) between turbine stages increases power, and during operation with high pressure ratios or with applying heat regeneration, efficiency as well. Applying intercooling, heat regeneration and sequential combustion, Fig. 1.b, enables the gas turbine cycle to approach the Ericsson cycle. An ideal Ericsson cycle consists of isothermal compression and expansion processes, combined with isobaric heat regeneration between them. The thermal efficiency of the ideal Ericsson cycle equals to the Carnot efficiency, the maximum efficiency for a thermal power engine operating between two temperature levels.

The rotating components of a gas turbine in stationary service are normally connected to one, two or three shafts. The single shaft arrangement is inherently the simplest form by virtue that its structure has the compressor, turbine and load interconnected. Twin shaft arrangements may have high pressure components rotating as one unit and the low pressure components together with the load as the other. During operation with high pressure ratios, this reduces the risk of axial compressors surging at part-load duty. Another arrangement of twin shaft engines is to have the compressor and the high pressure turbine interconnected as a gas generator and the low pressure turbine with the load as a free power turbine. Compared to single shaft arrangements, this gives added flexibility for part-load operation. However, the risk of overspeeding due to loss of load is evident. Triple shaft arrangements have usually low and high pressure components connected accordingly to low and high pressure shafts, a free power turbine rotating the third shaft with the load.

Industrial scale gas turbines can be divided into two main categories: engines primarily designed for industrial use and gas turbines derived from jet engines. Modifying a jet engine for industrial purposes comprises the installation of a free power turbine to replace the propulsive nozzle. Compared to industrial gas turbines, aeroderivative engines commonly feature a better efficiency and higher power-to-weight ratio resulting from a more sophisticated construction and technology level. With none of the previously mentioned additions (intercooling, sequential combustion and heat regeneration) to the basic cycle, the efficiency may be up to 42 % (LHV) and power up to 50 MW. However, aerotechnology is becoming increasingly adapted in current industrial gas turbine design as well so as to further the utmost efficiencies of the basic cycle to values exceeding 38 % (LHV). Unit sizes and performances of industrial gas turbines have been under constant improvement too, the maximum values currently exceeding 250 MW. Industrial gas turbines mainly apply single and twin shaft configurations.

Gas turbines have a significant role in modern society. In traffic they serve as a mover, besides aeroplanes, on high speed ferries for instance. Power production employs aeroderivative engines, especially for peak load use and reserve power on account of their light weight and start-up capabilities. Industrial and heavy frame gas turbines are more adequate for base load operation in, for example, combined heat and power production. In industry, gas turbines have several applications for mechanical energy generation, for offshore platform use and driving gas compressors, for instance.

2.2 Cycle configurations under study

This study concentrates on three main configurations as illustrated in Fig. 2, all of which are based on the open gas turbine cycle with internal combustion. As the simplest case, Fig. 2.a portrays a single shaft arrangement, typical of industrial and heavy frame gas turbines. Figure 2.b represents the layout of frequently used older aeroderivative applications where the propulsive nozzle has been replaced by a separate power turbine, thus constituting a twin shaft engine. Another configuration of multiple shaft gas turbines may be seen in Fig. 2.c, which was inspired by the Collaborative Advanced Gas Turbine development programme. This programme aims to accelerate the commercial availability of higher efficiency (60+ % LHV), natural-gas-fuelled advanced gas turbines for electric power generating applications in the next decade. An important intermediate

goal of the programme is to develop and demonstrate intercooled aeroderivative (ICAD) gas turbines based on existing high-thrust aircraft engines, thus raising the efficiency of simple cycles up to 45–47 % (LHV).

All of the configurations presented above may be equipped with a heat exchanger as shown in the layouts in Figures 2.d–f, to regenerate the heat from the turbine discharge gas. A plate-fin recuperator of counterflow arrangement has been selected for this model. Cooling the air for turbine blade cooling purposes is optional too, and may be implemented either by the use of water or ambient air. Intercooling between the compressor stages in Figs. 2.c and 2.f can also be accomplished either with water or with ambient air.

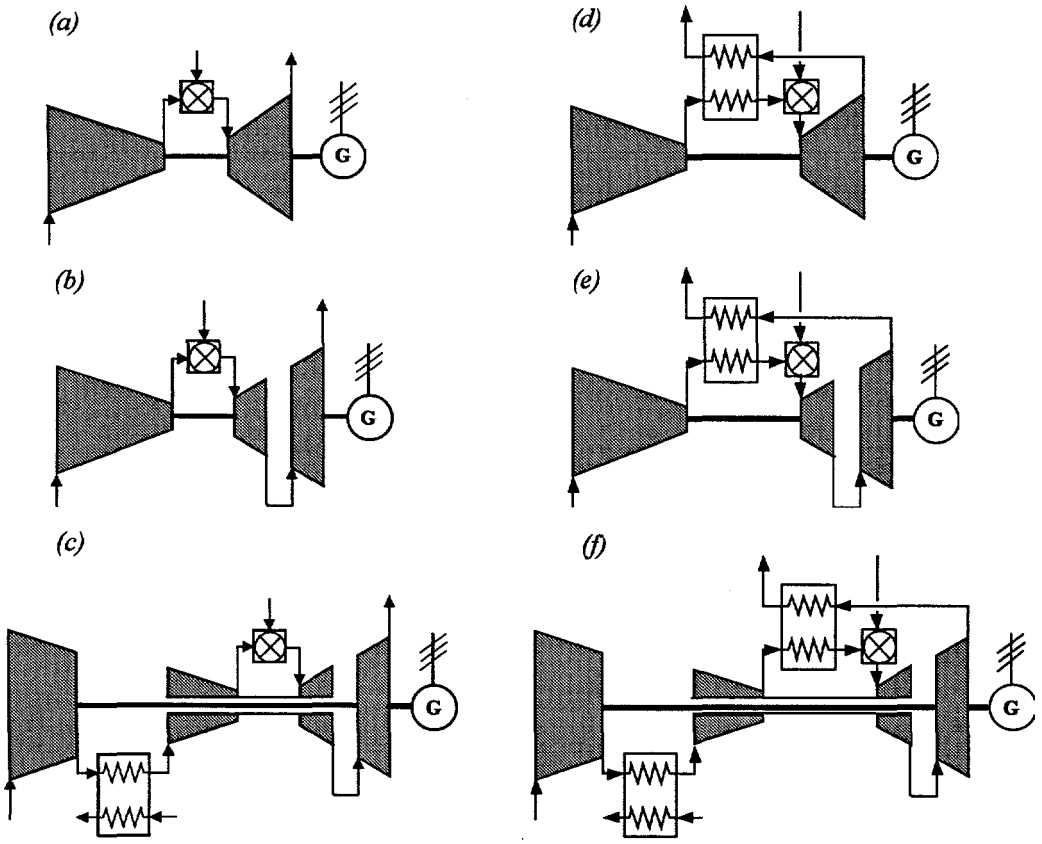

Figure 2. Schematics of examined gas turbine configurations for use in utility applications.
a) single shaft gas turbine *b)* twin shaft gas turbine with detached power turbine *c)* twin shaft intercooled gas turbine, generator typically in high pressure shaft *d–f)* corresponding engines with heat regeneration

3 REVIEW OF THERMODYNAMICS

The behaviour of gas turbine components can be determined with a few thermodynamic definitions. Yet these basics are frequently overlooked and used without closer consideration of their fundamentals, inducing thus potential risk of misuse. Therefore, these aspects are briefly surveyed in this chapter.

3.1 The perfect gas model

Gas is a composition of randomly moving particles: molecules, atoms, ions and electrons for instance, which all are affected by the ambient electric sphere of activity. These intermolecular forces influence the motion of the particles and hence the thermodynamic properties of gas, since the thermodynamic behaviour is no more than a derivative of the molecular state.

The perfect gas model assumes that the molecular volume of gas, and thereby the mean distances of the particles, is high enough for the intermolecular forces to be neglected. The equation of state is thus, as given by Moran et al. [1993]

$$p v = R T \tag{3.1}$$

Consistent with prevailing policy in gas turbine calculations, the specific gas constant will be used, defined as the ratio of the universal gas constant to the molecular mass of the gas. In comparison with applying the universal gas constant, this results in a significant simplification of the calculation routines.

The perfect gas model can be applied if the temperature of the gas is considerably beyond its critical temperature and the pressure below the critical pressure[1]. According to Reynolds [1979], for air for instance, the critical values are 132.5 K and 37.7 bar, for combustion gases CO_2 and H_2O (from hydrocarbon fuel) 304.2 K, 73.8 bar and 647.3 K, 221 bar, respectively. Hence, pressures and temperatures generally occurring in gas turbine cycles justify the use of the model. The accuracy of

[1] It should be noted that the model must not be applied at a temperature level high enough to enable dissociation reactions in gas, i.e., reduction of molecules into atoms. According to Anderson [1990] however, with atmospheric air for instance, dissociation does not occur at temperatures below 2500 K.

the perfect gas assumption is also reasonably high, the maximum error of pressure for air was detected by Larjola [1982] to be 0.4 % in the pressure range 1–10 bar and 1.9 % in the range 1–50 bar. The temperature range for the calculations was 323–1300 K. Low temperatures and high pressures rarely occur simultaneously in a gas turbine cycle, thus improving the validity of the model.

The combustion gases contain water vapour - as products of combustion and due to humidity. However, the partial pressure of steam is low and temperature high, therefore the perfect gas model can also be applied here.

Specific enthalpy can be defined as by Moran et al. [1993]

$$h = u + p\,v \tag{3.2}$$

According to Gibb's law, the enthalpy of a gas system at equilibrium can be determined by two independent state variables, temperature and pressure for instance, thus for enthalpy and its derivative

$$h = h(T,p) \tag{3.3}$$

$$dh = \left(\frac{\partial h}{\partial T}\right)_p dT + \left(\frac{\partial h}{\partial p}\right)_T dp \tag{3.4}$$

According to the perfect gas model, the product of pressure and specific volume vary with temperature only. So also does internal energy and consequently specific enthalpy. The equations above can therefore be simplified to

$$h = h(T) \tag{3.5}$$

$$dh = \left(\frac{\partial h}{\partial T}\right)_p dT \tag{3.6}$$

The partial derivative which remains is the definition of isobaric specific heat capacity. Hence, the difference of enthalpy for a perfect gas may be expressed as

$$dh = c_p(T)\, dT \tag{3.7}$$

According to the First Law of Thermodynamics, the internal energy of a system varies only with energy transfers – work and heat – between the system and its surroundings[1] as

$$du = \delta q + \delta w \tag{3.8}$$

The Second Law states that the entropy of an isolated system either remains constant or increases. The difference of entropy for the system at equilibrium can be classified resulting from heat transfer and dissipation, generated by friction for instance

$$ds = ds_q + ds_w \tag{3.9}$$

Heat and work, which consists of an alteration of volume and frictional resistance, can be defined as

$$\delta q = T ds_q \tag{3.10}$$

$$\delta w = -p\,dv + T\,ds_w \tag{3.11}$$

Combining the equations gained from the First and Second Laws gives the Gibb's equation as

$$T ds = du + p\,dv \tag{3.12}$$

Differentiating the definition for specific enthalpy yields $dh = du + p\,dv + v\,dp$, enabling the entropy difference from the above equation to be written as

$$ds = \frac{dh - v\,dp}{T} \tag{3.13}$$

By applying the perfect gas model and substituting $dh = c_p(T)\,dT$, the difference of entropy can be further developed to indicate that it varies with both temperature and pressure as

$$ds = c_p(T)\frac{dT}{T} - R\frac{dp}{p} \tag{3.14}$$

All the gaseous substances of a gas turbine cycle - air, combustion gases and fuel gas - are mixtures of components. Yet, the consideration given here applies to gas mixtures as well. The specific properties are thus attained by weighting by the mass fraction of the components, the molecular properties accordingly by weighting by the mole fractions.

---

[1] Internal energy, *u*, is a state variable, therefore *du* varies only with the initial and end states of the system, not with the process between. Instead, δq and δw vary with the process.

3.2 Total state values

The actual conditions of a flowing gas, defined by pressure and temperature, are referred to as static state, and consequently static pressure, static temperature and static enthalpy. Imagine having the flow decelerated to rest isentropically[1], the conditions thus attained are referred to as total (stagnation) state and total state values, accordingly. Therefore, from the point of view of a gas flow itself, this total state concept is merely imaginary.

Total enthalpy can be defined as by Traupel [1966]

$$h_t = h + \frac{1}{2} w^2 \tag{3.15}$$

For a perfect gas, an approximate relation between total enthalpy and total temperature can be derived by integrating the equation $dh = c_p \, dT$ and assuming that the specific heat capacity is constant. The error thus arising will be minimised using the value for heat capacity at an average temperature of $(T_t + T)/2$.

$$h_t = h + \bar{c}_p (T_t - T) \tag{3.16}$$

With the definition of total enthalpy Eq. (3.15), the relation between static and total temperature can be established as

$$T_t = T + \frac{w^2}{2\bar{c}_p} \tag{3.17}$$

The relation between static and total pressures can be obtained by setting the difference of entropy equal to zero in Eq. (3.14) and by integrating the equation thus formulated. Again, the specific heat capacity has been assumed to be constant.

$$p_t = p \left(\frac{T_t}{T} \right)^{\frac{\bar{c}_p}{R}} \tag{3.18}$$

---

[1] According to Anderson [1990], total temperature and total enthalpy assume only an adiabatic (thermally isolated), not necessarily isentropic process. This does not, however, affect the theorems in this study.

By combining the two above equations, total pressure can be determined with static state values as

$$p_t = p\left(\frac{w^2}{2\bar{c}_p T}+1\right)^{\frac{\bar{c}_p}{R}} \tag{3.19}$$

The use of total state values in turbomachinery is reasonable due to their simplification of the calculation, as will be shown next. However, in this thesis the primary goal has been the general validity of the model, therefore the use of total state values has been omitted by presuming that the cycle points are located so that the gas velocity remains low (< 50 m/s). Then static and total states can be approximated as being equal and no information regarding the gas velocities or the structural dimensions of the gas turbines is required.

3.3 The energy balance

The energy balance is the foundation of all thermodynamic flow processes - it is formed using the First Law of Thermodynamics. Consider a differential mass *dm* flowing in a steady state flow system bordered by the control volume boundary, as illustrated in Fig. 3. Between the cycle points 1 and 2, mechanical power, P, is introduced into the process and heat, Φ, is released from it. Pressures p_1 and p_2 produce work to the amount of $(p_1 v_1 - p_2 v_2)\, dm$.

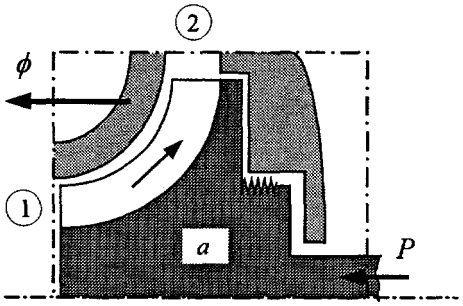

Figure 3. The energy balance applied to the impeller, *a*, of a radial compressor.

Energy transfer between the control volume and the surroundings consists of heat, mechanical work and volumetric work. Hence, the right-hand side of the equation $dU = \delta Q + \delta W$ (which applies from the First Law of Thermodynamics) becomes

$$\delta Q + \delta W = \Phi\, dt + P\, dt + (p_1 v_1 - p_2 v_2)\, dm \tag{3.20}$$

While the co-ordinates are fixed off the system, the alterations in kinetic energy and potential energy have to be taken into account on the left-hand side of the equation $dU = \delta Q + \delta W$, thus

$$(u_2 - u_1)\, dm + \left(\frac{w_2^2 - w_1^2}{2}\right) dm + g(z_2 - z_1)\, dm = \Phi\, dt + P\, dt + (p_1 v_1 - p_2 v_2)\, dm \tag{3.21}$$

With the definition of enthalpy $h = u + pv$, the equation above can be developed to state the energy balance as

$$P + \Phi = q_m \left(\Delta h + \frac{\Delta w^2}{2} + g \Delta z\right) \tag{3.22}$$

Heat transfer between the gas and the surrounding flow channel remains negligible in turbines and uncooled compressors, therefore the system can be treated as adiabatic with reasonable accuracy. Alterations in potential energy can be omitted as well, allowing the energy balance for compressors and turbines to be presented with total state values simply as

$$P = q_m \Delta h_t \tag{3.23}$$

3.4 Expansion and compression processes

A universal means of rating processes is to compare the amount of work of an actual process to that of an ideal process. According to Wilson [1988], the reference process for adiabatic compressors and turbines is generally isentropic, thus producing isentropic (or adiabatic) efficiency. Furthermore, as a limit of isentropic efficiency for pressure ratios approaching unity, polytropic (or small stage) efficiency is frequently used.

With the aid of an energy balance, the definition for isentropic efficiency can be presented as

$$\eta_{sk} = \frac{P_s}{P} = \frac{\Delta h_{ts}}{\Delta h_t} \qquad \text{for compression} \qquad (3.24)$$

$$\eta_{st} = \frac{P}{P_s} = \frac{\Delta h_t}{\Delta h_{ts}} \qquad \text{for expansion} \qquad (3.25)$$

In accordance with the equation for total pressure, for an isentropic process the difference of entropy in Eq. (3.14) may be set to zero. If we then integrate the equation thus obtained, and assume that the specific heat capacity remains constant, the well known equation for isentropic processes is given

$$\frac{T_2}{T_1} = \left(\frac{p_2}{p_1}\right)^{\frac{R}{\bar{c}_p}} \qquad (3.26)$$

The constant heat capacity assumption is reasonably accurate in this context if it is evaluated at its mean temperature, $(T_t + T)/2$. For instance, the error arising due to the use of a constant heat capacity on calculating the end temperature for air remains below 0.01 %, for a pressure ratio of 2.5 and an initial temperature of 423 K.

In multistage compressors and turbines, the isentropic efficiency varies not only with the losses in the process, but also with the pressure ratio. In compressors, the efficiency decreases with an increase in pressure ratio, resulting from the increase in temperature, volume and consequently in the work needed for compression. In turbines, the phenomena occur to the contrary.

The influence of the pressure ratio will vanish on employing the isentropic efficiency for a differentially small process - the polytropic efficiency. According to Eq. (3.13), the enthalpy difference in an isentropic process can be expressed as $dh_s = v\,dp$, therefore the definition for polytropic efficiency can be written as

$$\eta_{pk} = \frac{dh_s}{dh} = \frac{v\,dp}{dh} \qquad \text{for compression} \qquad (3.27)$$

$$\eta_{pt} = \frac{dh}{dh_s} = \frac{dh}{v\,dp} \qquad \text{for expansion} \qquad (3.28)$$

Substituting $dh = c_p\, dT$, applying the perfect gas model and integrating the equations with a constant heat capacity, the expressions for a polytropic process become

$$\frac{T_2}{T_1} = \left(\frac{p_2}{p_1}\right)^{\frac{R}{\bar{c}_p \eta_{pk}}} \qquad \text{for compression} \qquad (3.29)$$

$$\frac{T_2}{T_1} = \left(\frac{p_2}{p_1}\right)^{\frac{R\eta_{pt}}{\bar{c}_p}} \qquad \text{for expansion} \qquad (3.30)$$

The specific heat capacity must be evaluated at its mean temperature here, too.

Since the polytropic efficiency is independent of the pressure ratio, it can be applied for comparing gas turbines with different values of pressure ratio. The use of the polytropic efficiency also simplifies the analysis of the gas turbine cycle, since component efficiencies can be fixed while varying the design value for the pressure ratio. As a consequence, the use of the polytropic efficiency instead of the isentropic efficiency should be preferred.

The relation between isentropic and polytropic efficiency can be presented with the following equations

$$\eta_{sk} = \frac{\Delta h_{ts}}{\Delta h_t} \cong \frac{\left(\frac{p_{t2}}{p_{t1}}\right)^{\frac{R}{\bar{c}_p}} - 1}{\left(\frac{p_{t2}}{p_{t1}}\right)^{\frac{R}{\bar{c}_p \eta_{pk}}} - 1} \qquad \text{for compression} \qquad (3.31)$$

$$\eta_{st} = \frac{\Delta h_t}{\Delta h_{ts}} \cong \frac{1 - \left(\frac{p_{t2}}{p_{t1}}\right)^{\frac{R\eta_{pt}}{\bar{c}_p}}}{1 - \left(\frac{p_{t2}}{p_{t1}}\right)^{\frac{R}{\bar{c}_p}}} \qquad \text{for expansion} \qquad (3.32)$$

The specific heat capacities of the isentropic and the actual process differ slightly causing inequalities in the equations above. However, in practice, this error is small. For instance, compressing air with an initial temperature of 300 K and a polytropic efficiency of 0.85, the use of Eq. (3.31) produces a relative error of 0.1 % with a pressure ratio of 10.

As noted by Wilson [1988], the end pressures in the equations introduced here should agree with the definition of the appropriate efficiency. The pressure may have been taken after the diffuser, for instance. Total state values – or more precisely, total-to-total state values – are frequently applied when the kinetic energy of the gas can be utilized in the next stage. For the opposite case, the static end pressure (total-to-static) is normally applied, but not static end temperature however.

4 GAS TURBINE COMPONENT MODELS

Modelling the design operation of gas turbine components is a simplicity, though not a triviality – principally, it is no more than a synthesis of the thermodynamic principles formerly introduced. Yet, it is also a basis for off-design modelling. The alteration of mass flows, pressure ratios and various losses outside the design state merely determine the transition of the equilibrium from design operation to off-design. This chapter presents an extension of the thermodynamic aspects, with respect to the special features of each component.

4.1 The compressor

The role of the compressor is to increase the pressure of air. The energy transfer into air required in this process is implemented by the rotor, increasing the velocity of air flowing through the rotor passages. In the rotor stage, the increase in pressure is due to a decline in velocity proportional to the rotor blade speed, while in the stator stage the kinetic energy of the gas is converted into a pressure rise. The number of consecutive rotor-stator stages may be in excess of 20 for axial compressors operating with high pressure ratios.

4.1.1 Performance maps

The rotational speed and mass flow of the compressor generally differ from their design value, thus altering the efficiency and pressure ratio produced. For characterisation with compressor maps, these relations may be determined analytically, as given by Attia et al. [1995] for multistage compressors using compressor geometry and the design point data for instance, but are usually acquired from test measurements. Representation of the maps vary – a general, though not universal means, is to plot mass flow and efficiency against pressure ratio – and they may be valid for a definite inlet temperature and pressure only. General validity can be achieved by applying aerodynamic similarities, as by Traupel [1966], or by a dimensional analysis, as by Dixon [1984]. The former is given here, to present all flow conditions of a similar type as one point on a plane.

Consider a multistage compressor of the axial type, the performance map presenting an abscissa of relative mass flow q_m/q_{m0} and ordinates of pressure ratio π and efficiency η, the curve parameter

being the relative speed of rotation N/N_0 (the subscript 0 referring to the design values). The aerodynamic similarity between any two operational states will be fulfilled by requiring that relations of flow velocities between the states remain constant throughout the compressor.

The requirement of equality of pressure ratios between the states provides equality of temperature ratios as well, since similar conditions may be assumed to produce similar efficiencies and, within reasonable accuracy, the specific heat capacity can be assumed constant too[1]. Denoting the reference state with the subscript *ref*, therefore, for the temperature ratio, it applies

$$\frac{T_{i+1}}{T_{i+1\,ref}} = \frac{T_i\left(\frac{p_{i+1}}{p_i}\right)^{\frac{R}{\bar{c}_p\eta_p}}}{T_{i\,ref}\left(\frac{p_{i+1}}{p_i}\right)^{\frac{R}{\bar{c}_p\eta_p}}} = \frac{T_i}{T_{i\,ref}} \tag{4.1}$$

Due to constancy of pressure and temperature ratios, the relations of densities between the states also remain constant, which - based on continuance - is an adequate prerequisite for steadiness of velocity ratios, and for aerodynamic similarity.

A typical cross-section of the first stage of a multi-stage axial compressor is illustrated in Fig. 4. No work is transferred by the stator row, so the energy balance for the stator can be applied according to Eq. (3.23) as

$$h_2 + \frac{1}{2}c_2^2 = h_3 + \frac{1}{2}c_3^2 \tag{4.2}$$

By approximating the finite difference of enthalpy in the form $\Delta h = \bar{c}_p \Delta T$, using the polytropic equation (3.29) and substituting $c_3 = K\,c_2$, the above equation becomes

$$\frac{1}{2}c_2^2\left(1-K^2\right) = \bar{c}_p T_2\left[\left(\frac{p_3}{p_2}\right)^{\frac{R}{\bar{c}_p\eta_p}} - 1\right] \tag{4.3}$$

[1] The influence of humidity on the gas constant has been neglected in this context due its insignificance during operation near the standard ambient conditions (15 °C, 101.3 kPa, 60 % relative humidity). However, extreme deviations from these conditions affect, not only the gas constant, but the specific heat capacity as well, thus impairing the accuracy of this presentation.

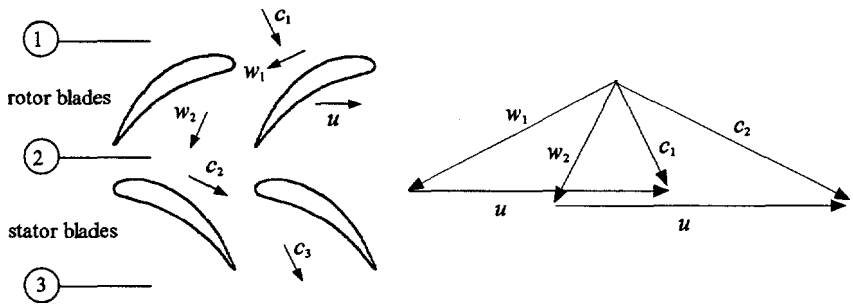

Figure 4. Typical cross-section of the first stage of a multi-stage axial compressor and the velocity triangles.

Apart from c_2 and T_2, two similar flow conditions have all the above terms equal, so for the relation of the velocities between the states, it follows that

$$\frac{c_2}{c_{2\,ref}} = \sqrt{\frac{T_2}{T_{2\,ref}}} \tag{4.4}$$

Based on similarity, the velocity ratio can be substituted for by the velocity ratio at the inlet plane, and based on Eq. (4.1) the temperature ratio can also be substituted for, thus

$$\frac{c_1}{c_{1\,ref}} = \sqrt{\frac{T_1}{T_{1\,ref}}} \tag{4.5}$$

The magnitude of the velocity of the incoming flow, c_1, varies with temperature and pressure, whereas its direction varies only with compressor geometry. Figure 4 shows, as an example, that the equality of the velocity ratios c_1/c_{1ref} and w_1/w_{1ref} applies only if the velocity triangles between the states are similar. This is if and only if $u/c_1 = constant$. Since the tangential velocity of the rotor blade u is proportional to the speed N, Eq. (4.5) can be presented as

$$\frac{N}{N_{ref}} = \sqrt{\frac{T_1}{T_{1\,ref}}} \tag{4.6}$$

Based on continuity, the ratio of mass flows through the compressor can be stated as

$$\frac{q_m}{q_{m\,ref}} = \frac{c_{n1}\, A_1\, \rho_1}{c_{n1\,ref}\, A_1\, \rho_{1\,ref}} \tag{4.7}$$

The constant A_1 is defined as the flow area at the rotor inlet. Due to similarity of the velocity triangles, the ratio of axial velocities c_{n1}/c_{n1ref} can be substituted for with the ratio c_1/c_{1ref}. Hence, applying Eq. (4.5) and the perfect gas model, the above equation can be presented as

$$\frac{q_m}{q_{mref}} = \sqrt{\frac{T_1}{T_{1ref}}}\frac{\rho_1}{\rho_{1ref}} = \sqrt{\frac{T_{1ref}}{T_1}}\frac{p_1}{p_{1ref}} \qquad (4.8)$$

Equations (4.6) and (4.8) determine the alteration of rotational speed and mass flow due to a change in inlet temperature and pressure so that the efficiency and pressure ratio produced by the compressor remain unchanged. With these equations, the compressor map can thus be generalised to apply for all inlet temperatures and pressures. The rotation term N/N_0 and mass flow term q_m/q_{m0} of the original map constitute the reference values N_{ref}/N_0 and q_{mref}/q_{m0}, into which N_{ref} from Eq. (4.6) and q_{mref} from Eq. (4.8) are to be substituted. As a result, the generalised forms for the terms become

- rotational speed *(Φ)* $\quad \frac{N}{N_0}\sqrt{\frac{T_{10}}{T_1}} \quad \left(\frac{N}{\sqrt{T_1}}\ \textit{relative to design value}\right)$
- mass flow $\quad \frac{q_m}{q_{m0}}\sqrt{\frac{T_1}{T_{10}}}\frac{p_{10}}{p_1} \quad \left(\frac{q_m\sqrt{T_1}}{p_1}\ \textit{relative to design value}\right)$

Figure 5 presents, as an example, one form of mass flow and efficiency maps for an axial compressor with a design pressure ratio of 6, as given by Traupel [1966]. Instead of the actual pressure ratio, the ordinate axis has the term Π, thus enabling the use of the maps for other pressure ratios as well.

$$\Pi = \frac{\pi - 1}{\pi_0 - 1} \qquad (4.9)$$

The form of the maps is heavily influenced by the design criteria of the compressor. One vital factor is the distribution of velocities in the flow passages and, consequently, the reaction degree of the compressor stages which is defined as the ratio of the isentropic enthalpy rise in the rotor to the isentropic enthalpy rise summed up in the rotor and in the stator. According to Korakianitis et al. [1994b] for instance, an axial compressor with the reaction degree of approximately 0.5, has usually a higher maximum efficiency than a compressor with a higher reaction, but the decline in efficiency outside the optimum is more significant.

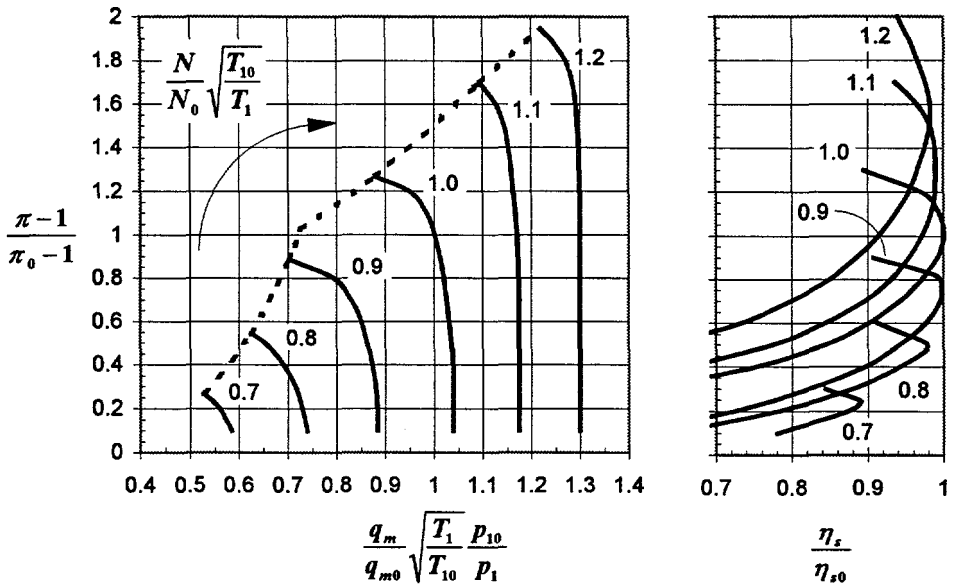

Figure 5. Typical maps for axial compressors with a pressure ratio of 4 to 8, presenting isentropic efficiency.

The prospective application of a gas turbine affects the choice of the design operating point on the compressor maps. The performance may be characterised by frequent part-load duty, hence justifying that the design values be located rather outside than at the optimum efficiency, as in Fig. 5. However, the transition of the operating point can easily be taken into account by dividing all the original terms of the map (the rotational term, pressure ratio, mass flow and efficiency terms) by the values gained from the new operating point.

From the point of normal operation in a gas turbine, the compressor maps feature two regions, separated by a surge line, as plotted by a dashed line in Fig. 5. With operating points far away from this line, normal operational conditions may be assumed to prevail. On approaching this surge limit at high speeds, the operation of the compressor becomes unstable. The compressor eventually surges with a further increase of pressure.

At the design conditions, all the compressor stages operate at the correct incidence (as determined by u/c_{n1} in Fig. 4). When moving towards the surge line, during design speed operation for instance, the density at the compressor exit will be increased due to the increase in discharge pressure while the mass flow will be reduced. This will reduce the axial velocity in the last stage

and correspondingly increase the incidence, thus causing the rotor blade to stall. Surging[1] is triggered by this stalling of the last stage, and subsequently cascading a stall back through the compressor.

Surging causes the mass flow to collapse and induces vibration that strains or even damages the construction. Therefore, the stable operation of the compressor is vital and the operating point is controlled so as not to move too close to the limit. The surge margin is defined with a pressure ratio at the surge line π_s, this being a function of the rotational term. The minimum value allowed for the surge margin is usually 0.1–0.2.

$$Y = \frac{\pi_s - \pi}{\pi} = \frac{\Pi_s(\pi_0 - 1) + 1 - \pi}{\pi} \tag{4.10}$$

The choking of flow is also featured on compressor maps. Decreasing the pressure ratio at normal operating conditions will, down to a certain limit, increase the mass flow and, consequently, the gas velocity. The maximum value of the mass flow parameter ($q_m\sqrt{T_1}/p_1$) will be reached at a pressure ratio which produces choking conditions. Choking refers to when the gas reaches sonic velocity at the limiting flow area in the compressor. In Fig. 5 for example, this can be seen by the constant speed parameter ($N/\sqrt{T_1}$) curves turning vertical. Extra mass flow through the compressor can then be gained only by higher speeds[2]. Choking is not harmful for the compressor in any way. However, the operating zone of gas turbines normally lies in the region of unchoked conditions for the sake of better efficiency.

4.1.2 Variable compressor geometry

Modern gas turbines implement two load control schemes: affecting the turbine inlet temperature and, consequently, power via the fuel flow, and altering the air flow via adjustment of the compressor inlet guide vanes. Combining the methods for power reduction normally incorporates the correspondence of the opening angle of the blades and power, down to a certain power limit, thus reducing the mass flow and the pressure ratio (and to some extent, the efficiency). As a

[1] True surging occurs only at high speeds. At low speeds the density will be lower than the design value. However, the mass flow generally falls off more rapidly, thus causing the axial velocity in the first stages to decrease and, correspondingly, the incidence to increase. As a result, at low speeds the front end of the compressor stalls – without normally causing surge.

[2] This additional mass flow will be limited by the ability of the diffuser area to accept the flow.

consequence of this, the air-to-fuel ratio remains favourable considering the formation of nitrous oxides and carbon monoxides on part-load operation as well. The turbine outlet temperature can also be held constant, which contributes to the operation of the heat recovery cycle after the gas turbine. By applying the variable compressor characteristics, the decrease in turbine inlet temperature on part-load operation will be reduced, thus improving part-load efficiencies of the gas turbine – despite the decrease in the pressure ratio.

Typical for modern gas turbines, 1–4 of the first compressor stages are equipped with adjustable stator cascades. The control mechanism of these blade rows is usually interconnected, so that the influence of the inlet guide vane control can be taken into account with maps that correspond to the characteristic blade setting angle, denoted here as β. In practice, satisfactory results can be expected to be gained using maps presented for three values of β only, selected to cover the expected area of variation. However, increasing the number of interpolation points is recommended. Hence, the terms for the mass flow and the efficiency of the compressor become functions of three variables: Φ, Π and β.

4.1.3 The use of simplified models

The overall performance of gas turbines is dominated by the compressor behaviour, therefore modelling gas turbine performance should always be primarily based on actual compressor characteristics. For most modern gas turbines on the market however, the component maps are propietary to the manufacturers and are not published.

Some simplified methods have been suggested to approximate the compressor behaviour outside design conditions, see Morchower [1995], for instance. However, without the information of compressor geometry, some vital performance data, such as the influence of variable stator blades or the surge margin, will be lost. For this reason, these methods should never be the first choice.

4.2 The combustion chamber

On operation between two pressure levels, the difference of enthalpy available to the turbine increases with an increase in the turbine inlet temperature. It is this distinct physical phenomenon that renders possible the operation of the gas turbine, and combustion chambers are used to execute this increase in temperature by burning fuel in the air flow. Aeroderivative engines use several combustion chambers of the can-annular type, whereas gas turbines of industrial design may be equipped with one or two chambers of the silo type instead. An alternative is to have numerous burners placed next to each other in one annular chamber.

Burning hydrocarbon based fuel - natural gas or fuel oil, for instance - produces mainly water vapour and carbon dioxide as emissions, but also nitrous oxides (NO_x), carbon monoxides (CO) and non-combusted hydrocarbons (HC). Apart from steam, all these emissions either pollute the air or accelerate the greenhouse effect. While the formation of carbon dioxide is inevitable due to combustion reactions, the quantities of NO_x , CO and HC compounds can be affected by combustion technology.

In conventional combustion chambers, the fuel was brought in, mixed with air and burnt with a diffusion flame simultaneously, thus inducing locally high temperatures and consequently nitrous oxides. The emission level of nitrous oxides with this type of combustion was generally to the magnitude of hundreds of ppmv. Until this decade, the primary means of reducing the NO_x emissions has been injecting water or steam into the combustion chamber, or using selective catalytic reduction. However, due to stringent environmental legislation, the emissions from gas turbines have become one significant design and marketing criterion producing new concepts for combustion processing. One approach is to have the fuel and air premixed prior to the combustion zone, combined with a lean air-to-fuel ratio and, therefore, lower temperature. Another application supplies fuel and air in three consecutive steps.

Advanced combustion chamber and burner technologies decrease the amount of nitrous oxides, as well as carbon monoxides and hydrocarbons, to a fraction of the conventional emissions level over a wide operational range of the gas turbine. This corresponds nearly 100 % combustion during part-load operation as well, since the amount of CO and HC emissions is inversely proportional to the efficiency of combustion. From the point of view of thermodynamic operation, combustion

reactions in modern gas turbines can thus be assumed ideal with reasonable accuracy over the majority of the operational range.

As an outcome to the foregoing discussion, the simplifications for the combustion chamber model in this study are as follows: The combustion chamber is considered adiabatic and hermetic. The combustion reactions are assumed ideal, thus the burning of hydrocarbons produces only carbon dioxide and water vapour, not carbon monoxide or non-combusted hydrocarbons. Small amounts of sulphur (from biogas, for instance) produce sulphur dioxide. Due to extremely low emissions of nitrous oxides, their formation is neglected.

In this model, the fuel may be selected from among fuel oil, natural gas, biogas or a mixture of chemical compounds. The set of components available consists of CH_4, C_2H_6, C_3H_8, C_4H_{10}, C_5H_{12}, C_2H_4, C_2H_2, C_6H_6, CO, CO_2, H_2, O_2, N_2, H_2O and H_2S presented by their mass or volume fractions. However, the composition must be determined by its chemical structure since elementary analysis itself does not enable the definition of heat capacities or heating values, for instance.

Combustion gases (referred to with the subscript *cg*) consist of products from stoichiometric combustion (*sg*) and the excess air (*a*) that is not participating in combustion reactions. Representing the amount of air required by stoichiometric combustion as L [$^{\text{kg air}}/_{\text{kg fuel}}$] , the energy balance for the combustion process may be applied as shown in Fig. 6. According to the standard ISO 2314: *Gas turbines - Acceptance tests* , the reference temperature is chosen to be +15 °C. The amount of air for cooling purposes has been referred to with the subscript *co*.

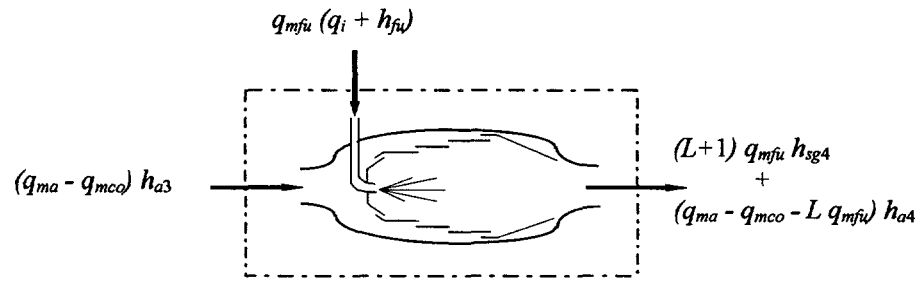

Figure 6. The energy balance of a combustion chamber.

According to the above figure, the amount of fuel for combustion can be determined as

$$q_{mfu} = \left(q_{ma} - q_{mco}\right) \frac{h_{a4} - h_3}{q_i + h_{fu} - (L+1)\, h_{sg4} + L\, h_{a4}} \tag{4.11}$$

The mass fraction of stoichiometric gases exiting the combustion chamber is

$$y_{cc} = \frac{(L+1)\, q_{mfu}}{q_{ma} - q_{mco} + q_{mfu}} \tag{4.12}$$

According to the energy balance, the calculation of combustion chambers should be executed with total state values. Yet, applying static state values does not affect the validity of the model since the flow velocities in the combustion chambers are low.

4.3 The turbine

Combustion gases expand in the turbine producing mechanical energy. The velocity of the gas flow is accelerated in the stator passages by the pressure gradient, and this kinetic energy is then converted into mechanical work in the rotor stages. Due to an increase in velocity proportional to the rotor blade speed, the pressure generally decreases in the rotor stages too. The number of consecutive stator-rotor stages in the axial turbines is usually 2–5.

Turbine inlet temperature has a crucial influence on the efficiency and specific power (thermal power divided by air mass flow at compressor inlet) of the gas turbine. Consequently, the development of gas turbines has been marked by striving towards higher turbine inlet temperatures[1]. Principally, the increase in temperature comes from improvements in materials technology introducing more heat resistant alloys, single-crystal structures and advanced coatings, as well as from advanced cooling techniques. As a result, the recent decades have seen an average of 20 °C annual increase in maximum inlet temperatures, currently placing turbine inlet temperatures in modern gas turbines in the range of 1500 K to 1800 K.

[1] Instead of increasing turbine inlet temperature, the efficiency of a gas turbine can also be improved by applying sequential combustion. One recently re-discovered implementation is to have two consecutive combustion chambers coupled by a single turbine stage.

4.3.1 Turbine cooling

Cooling turbine stages lowers the surface temperature of the blade material, thus enabling an immense increase – by hundreds of degrees Celsius – of turbine inlet temperature[1] with no reduction of the life span due to high-temperature creep or oxidation. Usually cooling air is first conducted through complex passages inside the blade, thus transferring heat by convection. The air exits through the surface of the blades, constituting a boundary layer that further cools and protects the blade from the hot combustion gases (film cooling). Due to high thermal stress, jet impingement cooling is often provided at the inside surface of the leading edge, thus cooling air coming up directly against the wall.

In addition to the first few turbine stages, cooling is normally applied to the annular walls of the hot gas path, and to the transition piece between the combustion chamber and the turbine as well. The total amount of cooling air is, in that case, typically 6–10 % of the total air mass flow entering the compressor.

The cooling of the hot-section alloys can be boosted, for instance, by cooling the compressor discharge air. Instead of air, steam has been utilised, especially for the stationary parts, to increase the cooling effect due its higher value of specific heat capacity. However this option is not included in this model.

The cooling air entering the flow region of the turbine lowers the average temperature of the combustion gases, and lowers the turbine efficiency due to the disturbance of the flows. Nevertheless, these disadvantages are offset by the increase in the maximum temperature – the combustion chamber exit temperature – in the optimum design.

Turbine inlet temperature is frequently determined according to the ISO 2314 standard. All cooling air is thus assumed to mix with the air prior the combustion chamber, consequently lowering the ISO-based turbine inlet temperature compared to the actual turbine inlet temperature[2] (average temperature of the combustion gases before the first stator stage). Another method presented by Traupel [1966] for estimating the influence of turbine cooling assumes the cooling air

[1] Manufacturers usually control the rotor inlet temperature of the first stage. Correspondingly, when a turbine is cooled, it enables a higher gas temperature to be used which is achieved by burning more fuel.
[2] The actual turbine inlet temperature is lower than the temperature of the combustion gases at the combustion chamber exit. This is due to cooling of the transition piece between the combustion chamber and the turbine.

to be mixed with the combustion gases before the turbine. Although the use of ISO-based turbine inlet temperatures for rating gas turbines is far more common and requires no information of the cooling air rate at this stage[1], the method of Traupel has been selected for this model. It enables changes in cooling air mass flow rate outside design operation to be taken into account as well. For demonstrative purposes however, the ISO-based turbine inlet temperature will be calculated in this model too.

According to Larjola [1982], for estimating the cooling air mass flow in an off-design region, the ratio of the compressor exit stagnation pressure to static pressure at the first turbine stage exit is usually high enough to justify the use of an equation for overcritical (choked) jet flow. Therefore, for the ratio of the cooling flows, applying only static values yields

$$\frac{q_{mco}}{q_{mco0}} = \frac{p_2}{p_{20}}\sqrt{\frac{T_{20}}{T_2}} \tag{4.13}$$

A recent study by Kim et al. [1995] has shown the benefits of coolant flow rate modulation in minimising the part-load efficiency degradation of gas turbine engines by reducing the losses caused by over-cooling turbine blades. It has not been used in this model, however.

According to the energy balance, the enthalpies corresponding to the ISO-based turbine inlet temperature and temperature by Traupel, denoted consequently as T_{4ISO} and T_{4M}, can be presented as

$$h_{4M} = \frac{\left(q_{ma} - q_{mco} + q_{mfu}\right) h_4 + q_{mco}\, h_{co}}{q_{ma} + q_{mfu}} \tag{4.14}$$

$$h_{4ISO} = \frac{q_{ma}\, h_3 + q_{mfu}\left(q_i + h_{fu}\right)}{q_{ma} + q_{mfu}} \tag{4.15}$$

In accordance with Eq. (4.12), for the mass fraction of stoichiometric combustion gases after cooling, it follows that

$$y = \frac{(L+1)\, q_{mfu}}{q_{ma} + q_{mfu}} \tag{4.16}$$

[1] Upon computation, the cooling air rate would be taken into account in determining the fuel flow.

Due to pressure losses, the pressure of the cooling flow and that of the combustion chamber exiting gas have both decreased. From the point of view of this model, the difference of these pressure losses is insignificant, and they have been assumed equal here. In practice, the pressure of the cooling flow must nevertheless be higher in order to facilitate the mixing of the flows. The use of booster fans may thus be necessary.

4.3.2 Turbine mass flow characteristics and the ellipse law

Turbine off-design performance can be accurately modelled - according to compressors - either with the use of turbine maps, or by calculating it on the grounds of turbine geometry as presented by Horlock [1985] and Schobeiri et al [1992] for instance. Since the availability of either is often poor, an approximation of the mass flow through the turbine is implied in accordance with Traupel [1966]. This gives reasonably good correspondence, especially for multi-stage axial turbines near the design conditions. Using the ellipse law, universal applicability of the model can also be preserved.

Firstly, let us examine the general speed characteristics of an axial flow turbine. According to compressor maps, pressure ratio is usually plotted against the mass flow parameter ($q_m\sqrt{T_4}/p_4$) for lines of the constant speed parameter ($N/\sqrt{T_4}$). The subscript 4 here denotes turbine inlet conditions. Increasing the pressure ratio will increase the mass flow up to a certain limit. The maximum value of $q_m\sqrt{T_4}/p_4$ will be reached at a pressure ratio which produces choking conditions at some point in the turbine. Usually, choking occurs in the stator nozzle blades or inlet casing[1]. In this case the constant speed lines converge to a single vertical line, as indicated in Fig. 7. The separation of the lines is typically moderate in the unchoked region of operation. Furthermore, increasing the number of stages will decrease the effect of speed on the mass flow, and make the representation of the mass flow characteristics by a single curve more accurate.

[1] If choking occurs in the rotor blade passages or in the annulus at the outlet from the turbine, the maximum mass flow will vary slightly with $N/\sqrt{T_4}$.

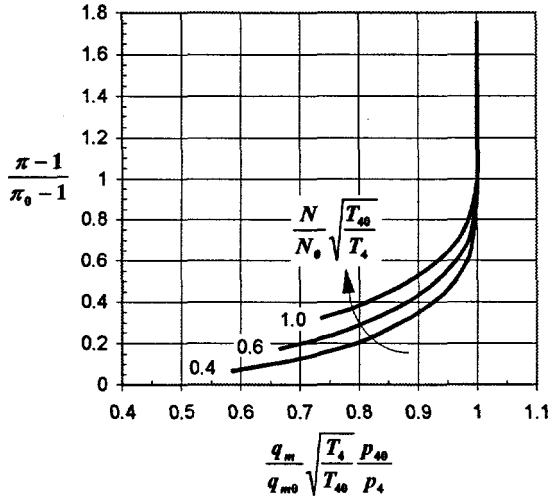

Figure 7. A typical mass flow map for a turbine, where the choking occurs in the stator nozzle blades or inlet casing.

To derive the ellipse law, consider an axial turbine with an infinite number of stages operating between points 4 and 5. Values for a single (arbitrary) stage exit will be referred to with the subscript *i*. Based on continuity, the mass flow through the stage can be written as

$$q_m = \frac{A_i\, c_{ni}}{v_i} \tag{4.17}$$

The ratio of the axial velocity to the (theoretical) velocity difference in the isentropic jet expansion defines the intake ratio $\mu_i = c_{ni}/\Delta c$. This varies with the blade geometry and flow conditions. Using the energy balance, the difference in velocity may be expressed with the isentropic enthalpy change as $\Delta c = \sqrt{2\,\Delta h_s}$, thereby Eq. (4.17) can be further manipulated as

$$\frac{q_m^2}{2\,\mu_i^2\,A_i^2} = \frac{\Delta h_s}{v_i^2} \tag{4.18}$$

According to Eq. (3.13), for infinitely small variations, the differential $dh_s = v\,dp$ applies. Consequently, for small pressure changes, this relation can be approximated as $\Delta h_s \approx v\,\Delta p$. Additionally, assuming the specific volume to remain constant throughout the stage $(v_i \approx v)$, Eq. (4.18) becomes

$$\frac{q_m^2}{2\,\mu_i^2\,A_i^2} = \frac{\Delta p}{v} \tag{4.19}$$

Suppose that expansion along the turbine conforms to a polytropic process, for which the equation of state can be presented as pv^n=*constant*. A relation between turbine inlet state and the actual state can thus be established as $v = v_4 \left(p_4/p\right)^{1/n}$. Substituting this into Eq. (4.19), denoting the ratio of p to p_4 as π, and the change in π as $\Delta\pi$, where $\Delta\pi = \Delta p/p_4$, yields

$$\frac{q_m^2}{2\,\mu_i^2\,A_i^2} = \frac{p_4}{v_4}\,\pi^{\frac{1}{n}}\,\Delta\pi \tag{4.20}$$

This equation applies for all turbine stages, thus summing up the equations for all the stages results in

$$q_m^2 \sum \frac{1}{2\,\mu_i^2\,A_i^2} = \frac{p_4}{v_4} \sum \left(\pi^{\frac{1}{n}}\,\Delta\pi \right) \tag{4.21}$$

Having assumed that the number of stages is high and therefore the pressure change per stage low, the summation on the right hand side of the equation may be approximated with an integral

$$\sum \left(\pi^{\frac{1}{n}}\,\Delta\pi \right) \approx \int_{\pi=\frac{p_5}{p_4}}^{\pi=1} \pi^{\frac{1}{n}}\,d\pi = \frac{n}{n+1}\left[1-\left(\frac{p_5}{p_4}\right)^{\frac{n+1}{n}} \right] \tag{4.22}$$

Furthermore, replacing the intake ratio for one stage with an appropriate term that represents the whole turbine and applying the perfect gas model, Eq. (4.21) can be presented in the form

$$\frac{q_m^2}{\mu^2} \sum \frac{1}{2\,A_i^2} = \frac{n}{n+1}\,\frac{p_4^2}{RT_4}\left[1-\left(\frac{p_5}{p_4}\right)^{\frac{n+1}{n}} \right] \tag{4.23}$$

The equation thus obtained applies for all conditions. Expressing it for two states, the other having design values (subscript 0) and dividing the equations hence formulated, an ellipse-law-like representation for the relative mass flow through the turbine is obtained

$$\frac{q_m}{q_{m0}} = \frac{\mu}{\mu_0}\sqrt{\frac{R_0}{R}}\,\frac{p_4}{p_{40}}\sqrt{\frac{T_{40}}{T_4}}\sqrt{\frac{n(n_0+1)}{n_0(n+1)}}\sqrt{\frac{1-\left(\frac{p_5}{p_4}\right)^{\frac{n+1}{n}}}{1-\left(\frac{p_{50}}{p_{40}}\right)^{\frac{n_0+1}{n_0}}}} \tag{4.24}$$

Except for the special case of a change in the type of fuel, the variation of the gas constant for the combustion gases is usually negligible. Therefore, the consideration of the term R_0/R in Eq. (4.24) is omitted.

The influence of turbine efficiency

Due to alterations in flow conditions, the exponent for polytropic expansion n does not remain constant throughout the turbine even though Eq. (4.22) assumes it so as to enable the integration. This does not however exclude the consideration of turbine efficiency and consequently the polytropic exponent differing between the states.

According to the equation pv^n=*constant*, for a polytropic process $p \propto (1/v)^n$. From Eq. (3.30) it may be seen that $p \propto T^{\bar{c}_p/(R\eta_p)}$. As for a perfect gas $v \propto T/p$, the relationship between polytropic efficiency and the exponent can be established as follows

$$p \propto \left(\frac{1}{v}\right)^n \propto \left(\frac{p}{T}\right)^n \propto \left(\frac{p}{p^{\frac{R\eta_p}{\bar{c}_p}}}\right)^n \propto \left(p^{\frac{\bar{c}_p - R\eta_p}{\bar{c}_p}}\right)^n \quad \Rightarrow \quad n = \frac{\bar{c}_p}{\bar{c}_p - R\eta_p} \qquad (4.25)$$

The behaviour of the turbine is dominated by its first stages, which can be noticed from the diminishing sums towards the end stages in Eq. (4.23) as well, due to the increasing cross-section of the flow passages. The value for the polytropic exponent in the ellipse law should therefore be selected on account of the front end of the turbine. In this context, no variation of the polytropic efficiency along the turbine is assumed, thus stage efficiencies are all alike and equal to the polytropic efficiency of the whole turbine.

The variation of the exponent in the operational region is insignificant, and so is its influence on the mass flow as given by Eq. (4.24). For instance, simultaneous changes in turbine inlet temperature from the design value of 1500 K to 1000 K, in polytropic efficiency from 0.85 to 0.70 and in pressure ratio from 6 to 4 correspond to a change[1] in the exponent from 1.24 to 1.21. In this case, substitution for the exponents for both states in Eq. (4.24) with the commonly used value of 1.3 will have an influence of only 0.3 % on the calculation for the mass flow. Therefore, the

[1] Combustion of fuel oil, and combustion gases with 80 mass-% of excess air was assumed.

consideration of the polytropic exponents is omitted in this model and the value of 1.3 is used universally.

The influence of rotational speed

The intake ratio, as well as efficiency, of an axial turbine stage vary with geometry and flow conditions – Traupel [1966], for instance, has presented variations of these terms as a function of blade speed ratio. For an axial flow turbine, it is defined as the blade speed at its mean height divided by the velocity equivalent of the isentropic enthalpy drop across the turbine stage $\nu = u/\sqrt{2\Delta h_s}$. The change in the intake ratio for a single stage and consequently for the whole turbine is small, hence the term μ/μ_0 has been excluded in this model. In practice the effect of rotational speed on the mass flow is determined by the reaction degree of the turbine, defined – according to the compressor – as the ratio of the isentropic enthalpy rise in the rotor to the isentropic enthalpy rise summed up in the rotor and in the stator. According to Wilson [1988], for impulse turbines having the enthalpy decreased in the stator only, the speed has little effect on the mass flow. For commonly used turbines with the reaction degree of approximately 0.5, it is more significant.

The influence of stage number

In previous considerations, the number of turbine stages has been assumed to be infinitely high. Normally the number of stages is below 5, thus impairing the accuracy of the ellipse law. Turbines having a finite number of stages may also be affected by choking of the flow due to an increase in pressure.

To estimate the magnitude of the stage number effect, consider the mass flow through a single-stage turbine. Decreasing the number of stages increases the pressure drop per stage (for similar initial and end states), so the enthalpy change in Eq. (4.18) can no longer be expressed with the specific volume and pressure drop. According to Eq. (3.7), the expression $\Delta h_s = \bar{c}_p \left(T_4 - T_{5s}\right)$ is used instead, with the specific heat capacity evaluated at its mean temperature. The order of the temperatures is reversed so as to retain the positive enthalpy change in accordance with Eq. (4.18).

According to Eq. (4.25), the term $R\eta_p/\bar{c}_p$ in the polytropic equation (3.30) equals $(n-1)/n$, thus for a polytropic expansion process $T \propto p^{(n-1)/n}$. For an isentropic process, a term that corresponds to n is denoted as k. Varying with temperature, it may be evaluated by setting $\eta_p = 1$ in Eq. (4.25). The equation for enthalpy change can thus be developed to be

$$\Delta h_s = \bar{c}_p T_4 \left[1 - \left(\frac{p_5}{p_4} \right)^{\frac{k-1}{k}} \right] \tag{4.26}$$

Using the assumption of a polytropic process, the specific volume at the turbine exit can be expressed with initial state values of $v_5 = v_4 \left(p_5/p_4 \right)^{-1/n}$. With the above equations, Eq. (4.18) can be generated to present the mass flow through the turbine as being

$$\frac{q_m^{\,2}}{2\mu^2 A_5^{\,2}} = \frac{\bar{c}_p T_4}{v_4^{\,2}} \left(\frac{p_5}{p_4} \right)^{\frac{2}{n}} \left[1 - \left(\frac{p_5}{p_4} \right)^{\frac{k-1}{k}} \right] \tag{4.27}$$

On account of the perfect gas model, T/v^2 equals $\left(p/R\right)^2 1/T$, and for an isentropic process $R/\bar{c}_p$ equals $(k-1)/k$. The term $\bar{c}_p T/v^2$ from Eq. (4.27) can thus be replaced by $k/(k-1)\, p^2/(RT)$. An expression for relative mass flow outside design operation can be established with this equation, by applying it for two states – the other having design values – and dividing the equations according to the procedure for the ellipse law. Terms for the intake ratio have been excluded accordingly and a value of 1.3 for polytropic exponent n has been used for both states. For the corresponding term k for an isentropic process, a value of 1.4 is chosen.

$$\frac{q_m}{q_{m0}} = \frac{p_4}{p_{40}} \sqrt{\frac{T_{40}}{T_4}} \sqrt{\frac{\left(\frac{p_5}{p_4} \right)^{\frac{2}{n}} \left[1 - \left(\frac{p_5}{p_4} \right)^{\frac{k-1}{k}} \right]}{\left(\frac{p_{50}}{p_{40}} \right)^{\frac{2}{n}} \left[1 - \left(\frac{p_{50}}{p_{40}} \right)^{\frac{k-1}{k}} \right]}} \tag{4.28}$$

Assuming isentropic flow, the exponents n and k may be set equal to each other and the equation applies for adiabatic jet flow[1] as well, as presented by Traupel [1966]. As a prerequisite, unchoked conditions are nevertheless required.

For gas flowing through a converging nozzle, the velocity of the flow at the throat will reach the speed of sound when the ratio of total pressure at the nozzle inlet to static pressure at the outlet has attained a value of $p_t/p = [(n+1)/2]^{n/(n-1)}$. Designated as the critical pressure ratio, this is the limit for the flow reaching choking conditions: with a further increase in pressure ratio, the flow velocity does not exceed the speed of sound at the throat. The precondition for a turbine with M stages to avoid choking of the flow is that pressure ratios at no stage will exceed the critical pressure ratio. Supposing all pressure ratios and polytropic exponents of actual turbine stages are equal, then the critical pressure ratio for the whole turbine would be the M:th power of the pressure ratio for the single stage. In practice, the pressure ratios vary between the stages, thus decreasing the value for the critical pressure ratio. According to Traupel [1966], increasing the reaction degree for the turbine stages has an increasing effect on the critical pressure ratio.

For an impulse turbine with a single stage, the critical pressure ratio is 1.832. A decrease of 15 % from this value will produce a difference of 7.3 % when comparing the results obtained with the ellipse law to the results given by Eq. (4.28). According to Traupel [1968], results converge rapidly when the number of stages and the reaction degree increases. Therefore the ellipse law can be used, for instance, in the modelling of the operation of a typical three stage turbine with reasonable accuracy.

Using the ellipse law does not enable the consideration of choking on actual gas turbines with a limited number of stages. However, from the point of normal operation, this is rather insignificant since gas turbines are generally designed to operate with unchoked conditions.

[1] One method of deriving the ellipse law is to examine a turbine with sequential impulse stages and to consider each stator passage as an adiabatic nozzle, as shown by Horlock [1985]. The kinetic energy from the nozzles is assumed to be transformed into mechanical work prior to the next stage, thus excluding the need for considering the energy of the incoming flow stage by stage. Fundamentally, the kinetic energy of the incoming flow may be supposed to pass through the turbine stage by stage for instance, having no influence on the calculation. In practice the velocity of the incoming flow however varies by stage, therefore deteriorating the assumption.

Resulting from the considerations given above for multi-stage turbines of the axial type, the variation of the mass flow outside design conditions can be modelled with the well-known ellipse law:

$$\frac{q_m}{q_{m0}} = \frac{p_4}{p_{40}}\sqrt{\frac{T_{40}}{T_4}}\sqrt{\frac{1-\left(\frac{p_5}{p_4}\right)^{\frac{n+1}{n}}}{1-\left(\frac{p_{50}}{p_{40}}\right)^{\frac{n+1}{n}}}} \qquad n = 1.3 \qquad (4.29)$$

For gas turbines with two consecutive turbines for instance, this ellipse law has to be applied separately for both turbines.

4.3.3 The efficiency map

The variation of the turbine efficiency outside design operation is significant and it is usually presented – similarly to the compressors – with maps. A general manner of representation is to plot efficiency against speed using various values for pressure ratio as the curve parameter. As an example, Fig. 8 illustrates a map presented by Traupel [1966] for a typical axial turbine. The abscissa of the map represents a rotational term $\Phi = N/N_0\sqrt{T_{\alpha 0}/T_\alpha}$ as a derivation from the blade speed ratio, the curve parameter being a universal term for pressure ratio as $\Pi = (\pi - 1)/(\pi_0 - 1)$ to enable the use of the map regardless of the design pressure ratio. The ordinate axis has been transformed to present isentropic efficiency relative to the design value. The subscript α refers to the inlet state of the turbine.

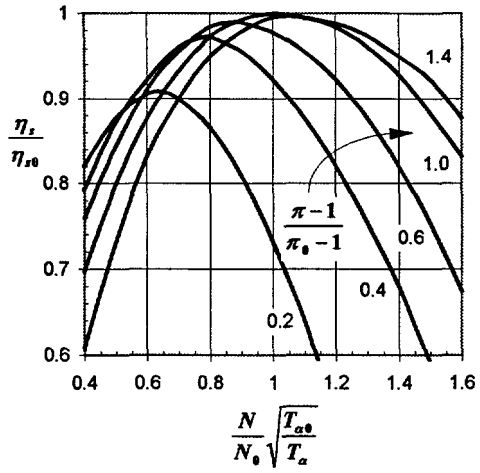

Figure 8. A typical efficiency map for axial turbines, plotting isentropic efficiency.

4.4 Heat exchangers

The efficiency of a gas turbine can be improved by utilising the heat from the turbine exhaust gas to heat up the compressor discharge air. The greater the temperature difference between the gas flows is, the better are the conditions for the heat exchangers to operate. Thus, employing heat regeneration is at its best with low pressure ratios and high turbine inlet temperatures.

Cooling the air, either during (or before) the compression, will increase especially the net energy available by reducing the work required for compression. While little gain in efficiency can be expected with connecting the intercooler to the basic (non-regenerated) cycle, the primary purpose for intercooling - along with the power increase - may be seen as the rise in the economically viable pressure ratio in the regenerative cycle by increasing the temperature difference between the gas flows. This will in turn benefit the efficiency and restrict the component sizes.

The third application for heat exchangers in this model arises from the desire for cooling the air that further cools the transition piece between the combustion chamber and the turbine, and the turbine blades themselves. This decreases the amount of air required for cooling purposes for the same firing temperatures, consequently increasing the compressor discharge air participating in the combustion process and improving the efficiency – or vice versa: it allows higher firing temperatures for the same gas turbine metallurgy thereby increasing the efficiency.

Based on the heat transfer phenomena, the heat exchangers used in regeneration may be classified as either recuperators or regenerators. While regenerators have a heat exchanger matrix exposed to either of the flows in turn, in recuperators air and combustion gases flow along their own passages and heat is transferred through the separating walls. A further classification of recuperators is based on the separating walls being of tubular and plate types. The principal arrangement of the flows may be against each other (counterflow), orthogonal (crossflow) or a combination of these.

Both the flows in heat exchangers are of gaseous form, for which the convective heat transfer – the transfer of heat between the wall and the medium – is poor, and the heat transfer surface required is thus large. In order to limit the size of the exchangers, a compact heat exchanger having a large heat transfer surface area per unit volume is a necessity. High surface densities can be achieved by using either finned plate recuperators with maximum values of approximately 5000 m^2/m^3, or regenerators with a compactness as high as over 10 000 m^2/m^3. For this study, a plate-fin recuperator of counterflow[1] arrangement is chosen for the sake of its prevalence. The flow channels may be fabricated using densely set parallel plates. These channels may incorporate fins that are pressed from thin metal sheets, so as to form triangular or rectangular shape by cross-section. Another approach is to form the separating plates to constitute the fin effect as well, thus eliminating the need for additional metal sheets and being consistently called primary surface design. Both these configurations have been outlined in Fig. 9.

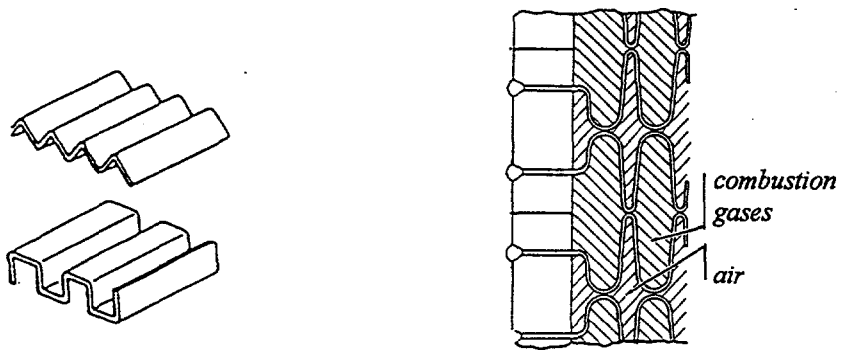

(a) *(b)*

Figure 9. Typical fin configurations for plate-fin recuperators using *a)* distinct sheet metal fins and *b)* primary surface design.

[1] The entry and exit sections are normally in crossflow for these heat exchangers. Due to their minor role in total heat transfer however, the counterflow theory can be applied to determine the overall performance of the exchangers.

The Reynolds number for a flow is defined as a ratio of inertial to viscous forces as by Incropera et al. [1990]

$$\mathrm{Re} = \frac{\rho w d_h}{\mu} = \frac{q_m d_h}{\mu A} \tag{4.30}$$

Due to a limit of the overall size, the flow channels of a typical heat exchanger are small, the hydraulic diameter of a single passage usually does not exceed 5 mm. In order to keep the pressure losses down, the flow velocities are also low. Therefore, according to Incropera et al. [1990], the Reynolds number remains moderate enough for the flow to be laminar.

Figure 10 shows the temperature distribution for a heat exchanger of counterflow arrangement. Instead of determining the efficiency of the exchanger as a ratio of the actual heat transfer rate to the maximum possible heat transfer rate, the term effectiveness (thermal ratio) of the heat exchanger is applied here, as by Cohen et al. [1987]. Denoted as ε, it is defined as the ratio of the temperature difference for the flow with the smaller thermal capacity to the maximum temperature difference available[1].

$$\varepsilon = \frac{T_3 - T_2}{T_6 - T_2} \tag{4.31}$$

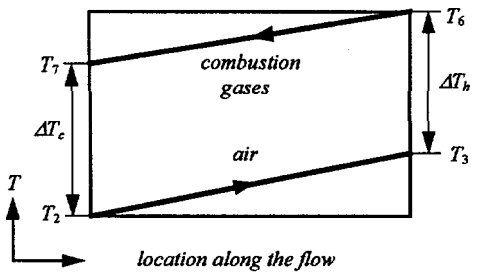

Figure 10. The temperature distribution in a counterflow heat exchanger.

[1] Using Eq. (3.7), the relationship between the efficiency, η, and the effectiveness, ε, of the heat exchanger becomes

$$\eta = \frac{\bar{c}_{pa\,2,3}}{\bar{c}_{pa\,2,6}} \varepsilon$$

The mean specific heat of air will normally not be very different over the two temperature ranges. Therefore, values for the effectiveness and for the efficiency are to a great extent alike.

4.4.1 Variation of the effectiveness

For estimating the effectiveness outside design operation, the actual temperature difference in the previous equation will be presented using a heat rate in accordance with the energy balance. Heat exchangers may be considered to be adiabatic, therefore heat is transferred only between the flows. Changes in potential and kinetic energy may also be neglected.

$$T_3 - T_2 = \frac{\Phi}{q_m \, \bar{c}_{pa}} \tag{4.32}$$

Expressing the effectiveness for two states (the other having design values denoted with a subscript 0), the ratio of the terms may thus be presented as

$$\frac{\varepsilon}{\varepsilon_0} = \frac{\Phi}{\Phi_0} \frac{q_{ma0}}{q_{ma}} \frac{\bar{c}_{pa0}}{\bar{c}_{pa}} \frac{T_{60} - T_{20}}{T_6 - T_2} \tag{4.33}$$

The heat transfer rate will be defined using the overall heat transfer coefficient, k. Due to the temperature difference of the flows altering across the exchanger, a logarithmic mean temperature difference (LMTD method) must be applied in this context.

$$\Phi = k \, A \, \Delta T_{\ln} \tag{4.34}$$

$$\Delta T_{\ln} = \frac{\Delta T_c - \Delta T_h}{\ln\left(\frac{\Delta T_c}{\Delta T_h}\right)} \tag{4.35}$$

In practice, heat is transferred in the recuperators via convection and conduction only. The role of radiation is negligible mainly on account of diminutive structural dimensions and low temperatures. The overall heat transfer coefficient of finned surfaces then applies universally as

$$\frac{1}{k \, A} = \frac{1}{\eta_{fa} \, A_a \, \alpha_a} + R_{mat} + \frac{1}{\eta_{fcg} \, A_{cg} \, \alpha_{cg}} \tag{4.36}$$

Transferring of heat from combustion gases to air is principally restrained by convection between the gases and the surfaces. Due to the high thermal conductivity and thinness of the materials, the conductive thermal resistance, R_{mat}, is a small fraction of the convective resistances, so it may be ignored. Therefore, a representation for overall heat transfer coefficient may be shown to be

$$k = \frac{\alpha_a}{1+\frac{\eta_{fa} A_a}{\eta_{fcg} A_{cg}} \frac{\alpha_a}{\alpha_{cg}}} \frac{\eta_{fa} A_a}{A} \tag{4.37}$$

The influence of the fins on the heat transfer rate – as taken into account by using the temperature effectiveness η_{fa} and η_{fcg} – depends not only on the fin material and structure, but also on the value of the overall heat transfer coefficient. These terms are nevertheless assumed constant through the operational range, as well as the ratio of the heat transfer coefficients α_a/α_{cg}. Using Eqs. (4.34) and (4.37), the ratio of the heat rates for the two states then becomes

$$\frac{\Phi}{\Phi_0} = \frac{\Delta T_{\ln}}{\Delta T_{\ln 0}} \frac{\alpha_a}{\alpha_{a0}} \tag{4.38}$$

To be able to determine the ratio of the heat transfer coefficients shown above, we need to consider further dimensionless numbers – the Nusselt number for characterising the total heat transfer proportional to molecular heat transfer, the Prandtl number for momentum with relation to thermal diffusivity and the Stanton number as a ratio of total heat transferred to total heat capacity.

The Nusselt number $$\mathrm{Nu} = \frac{\alpha d_h}{\lambda} \tag{4.39}$$

The Prandtl number $$\mathrm{Pr} = \frac{\mu \bar{c}_p}{\lambda} \tag{4.40}$$

The Stanton number $$\mathrm{St} = \frac{\mathrm{Nu}}{\mathrm{Re\,Pr}} = \frac{\alpha A}{q_m \bar{c}_p} \tag{4.41}$$

According to the definition of the Stanton number, the heat transfer coefficient can be written as

$$\alpha = \mathrm{St}\, q_m \bar{c}_p \frac{1}{A} \tag{4.42}$$

For the compact heat exchanger constructions illustrated in Fig. 9, fully developed laminar conditions may be assumed to prevail, the Nusselt number of the flow thus being constant. The variation of the Prandtl number for gases is normally small enough to be taken as a constant as well. According to Eq. (4.41), this yields $\mathrm{St} \propto \mathrm{Re}^{-1}$, hence, using the definition for the Reynolds number from Eq. (4.30), the ratio of the heat transfer coefficients may be shown to be

$$\frac{\alpha_a}{\alpha_{a0}} = \frac{\mu_a}{\mu_{a0}} \frac{\bar{c}_{pa}}{\bar{c}_{pa0}} \tag{4.43}$$

On manipulation of Eqs. (4.33), (4.38) and (4.43), for the ratio of effectivenesses, the following now applies

$$\frac{\varepsilon}{\varepsilon_0} = \frac{q_{ma0}}{q_{ma}} \frac{\mu_a}{\mu_{a0}} \frac{\Delta T_{\ln}}{\Delta T_{\ln 0}} \frac{T_{60} - T_{20}}{T_6 - T_2} \tag{4.44}$$

This model may be expected to give good results. In general, convective heat transfer in heat exchangers can be characterised using the Colburn factor for heat transfer analogy, j_H. It varies with the flow conditions and the structural design of the heat exchanger; for specific constructions it is extensively presented as a function of the Reynolds number by Kays et al. [1984], for instance:

$$j_H = \mathrm{St}\,\mathrm{Pr}^{2/3} = f(\mathrm{Re}) \tag{4.45}$$

For instance, on recuperators having a laminar boundary layer disrupted repeatedly – by dividing the rectangular fin forming sheets into strips transverse to the flow and by placing these strips so as to cause the flow to confront the edging of each strip – the Colburn factor can be shown to be $j_H \propto \mathrm{Re}^{-0.5}$, thus consequently $\mathrm{St} \propto \mathrm{Re}^{-0.5}$. Results gained with the corresponding model agree well with the results obtained by the more elaborated model with due consideration of the fins and the flow inlet/outlet guides, presented by Münzberg et al. [1977]. During operation with typical values, the difference of the results remained below 0.2 % at a part-load level of 60 %, for instance.

In the cases included in this study (Fig. 9), for the Colburn factor it applies that $j_H \propto \mathrm{St} \propto \mathrm{Re}^{-1}$, which has been seen from Eq. (4.41) as well.

The mass flows of air and combustion gases are almost equal and so are the corresponding heat capacities, hence the changes in temperature of each flow are almost alike too. Due to the definition of the logarithmic mean temperature difference, Eq. (4.35), divisions of infinitesimal numbers may therefore occur during computation of the process, consequently inducing run-time errors. This can be avoided however by substituting the logarithmic mean temperature difference with the (arithmetic) mean temperature difference defined as $\Delta T_m = 0.5(\Delta T_c + \Delta T_h)$. The error thus arisen will be small since the same transformation will be done on both sides of the quotient in Eq. (4.44).

It must be noted that for plate-fin recuperators, the application of the model for effectiveness, Eq. (4.44), is restricted to heat exchangers of the counterflow type only. Crossflow heat exchangers and types of combined crossflow-counterflow exchangers would require correcting the mean temperature difference with a factor, the value of which depends, not only on the structure of the exchanger, but also on the effectiveness and on the ratio of the heat capacity flows $\left(q_m \cdot c_p\right)$ as well. For instance, on a crossflow recuperator with unmixed flow, design effectiveness of 0.80 and ratio of heat capacities of approximately 1, decreasing the effectiveness by 10 % will increase the factor by 36 %. For diverse tubular heat exchangers the dependence of the Colburn factor on the Reynolds number will also frequently deviate excessively from the model.

Concerning the variation of the effectiveness, Eq. (4.47), this model can be applied to rotary regenerators. However, in doing this, one should take into account the cold-side and hot-side leakage flows from air into the combustion gases through wiping seals, as well as mechanical work required for rotating the heat transfer matrix.

4.4.2 The intercooler and cooling air cooler

Heat exchangers for cooling purposes commonly use water as the working fluid, if available, and are of a finned tubular configuration. This reduces the size of the exchangers and the heat thus gained can easily be recovered in the CHP process, for instance. In this model, the temperature of air at the heat exchanger exit is assumed constant regardless of the flow conditions. This approximation is universally satisfactory, but is especially valid for evaporative intercoolers[1]. Since cooling water is not included in the control volume, the outlet temperature of the air will be the only value required for both exchangers, along with the air-side pressure loss for the intercooler. If cooling would be accomplished using ambient air as a coolant, and a plate-type heat exchanger of counterflow arrangement for instance, the assumption that the variation of outlet temperature corresponds to Eqs. (4.31) and (4.44) would be appropriate for this case.

[1] The temperature difference between the fluids at the cold end varies only moderately even with major changes in operating conditions. The cooling water inlet temperature is usually constant as well.

4.5 Dissipative terms

The operation of an actual gas turbine is marked by the dissipation of energy. Each component having its surface temperature exceeding the ambient temperature, will be affected by heat losses to the surroundings. Due to isolation for instance, the heat flow is usually small enough to be neglected. Various irreversibilities – resulting from friction and single resistances for instance – will cause the pressure of the flowing gas to perpetually decrease. While included in compressor and turbine efficiencies already, the influence of pressure losses has to be taken into account elsewhere by using specific terms. Attention must also be paid to diverse mechanical losses originating from the bearings or from the transmission, and electric losses developed in the generator, if fitted.

4.5.1 Pressure losses

Before the compressor, a decrease in pressure will be induced by the intake channel, filtration and silencing systems for instance. Correspondingly, after the turbine pressure losses are induced by the exit channel, silencing systems and possible heat recovery unit. Pressure losses occur in combustion chambers and heat exchangers as well.

At design operation, the resistance of the flow will be taken into account by using terms for pressure loss relative to inlet pressure[1] (subscript α referring to the inlet state)

$$k = \frac{\Delta p}{p_\alpha} \tag{4.46}$$

The pressure losses are assumed to follow the well-known model for tubular flow as follows

$$\Delta p = \left(\xi \frac{l}{d_h} + \sum \zeta\right) \frac{1}{2} \rho_\alpha w_\alpha^2 \tag{4.47}$$

The flow of air and combustion gases is generally turbulent in the ducts and in the combustion chamber because of the wide channels combined with the low dynamic viscosity of the flow, thereby the dependence of the friction factor, ξ, on the state of the flow is weak. The term

[1] Total state values should be used with this context, however the use of static state values is justified on account of the assumption of low flow velocities.

containing factors for friction and single resistances in the the equation above is thus assumed to be constant outside design operation. Based on continuance and the equation of state for a perfect gas, the relative value for the pressure loss term outside design operation can be shown to be

$$\frac{k}{k_0} = \frac{p_{\alpha 0}}{p_\alpha}\frac{\rho_\alpha}{\rho_{\alpha 0}}\left(\frac{w_\alpha}{w_{\alpha 0}}\right)^2 = \frac{R}{R_0}\frac{T_\alpha}{T_{\alpha 0}}\left(\frac{p_{\alpha 0}}{p_\alpha}\right)^2\left(\frac{q_m}{q_{m0}}\right)^2 \tag{4.48}$$

According to Incropera et al. [1990] and Münzberg et al. [1977], modern compact heat exchangers typically have laminar[1] flow, augmenting the dependence of the flow resistance on the Reynolds number. For the sake of uniformity in this model, however, Eq. (4.48) has been applied for the pressure losses that are caused by recuperators and intercoolers as well. The error thus arising is insignificant.

Potential preheating to prevent the incoming air from freezing has been excluded from the control volume, thus the flow at the compressor inlet, as well as the flow at the turbine exit may be considered adiabatic. According to the energy balance, the pressure decreases isenthalpic and the temperature of the flowing gas remains unchanged.

4.5.2 Efficiencies

Mechanical losses will be taken into consideration in the form of a mechanical efficiency. For gas turbines with more than one shaft, terms for dividing the losses among these shafts are also needed. Subtracting the compressor power(s) from the turbine power(s) produces thermal power, and an additional subtraction of the mechanical losses will give us mechanical – or shaft – power.

$$P_{th} = \sum_i P_{ti} - \sum_i P_{ci} \tag{4.49}$$

$$P_{mech} = P_{th} - \sum_j P_{loss\,j} \tag{4.50}$$

$$\eta_{mech} = \frac{P_{mech}}{P_{th}} \tag{4.51}$$

$$z_j = \frac{P_{loss\,j}}{\sum_i P_{lossi}} \tag{4.52}$$

[1] Water-cooled intercoolers of a finned tubular configuration commonly have low Reynolds number turbulent flow.

For multi-shaft gas turbines, the energy balance for units without load can be stated as

$$P_{tj} = P_{cj} + P_{loss\,j} \tag{4.53}$$

Consequently, for twin shaft engines with free power turbines for instance, applying the energy balance to the high pressure turbine – compressor set will determine the thermodynamic state between the turbines. Also based on the energy balance, the shaft power for these engines can be presented in the form of

$$P_{mech} = P_{t2} - P_{c2} - P_{loss2} \tag{4.54}$$

Note that the above equations apply irrespective of the configuration of the twin shaft engines provided the components not existing in the corresponding unit will be set equal to zero. For instance, for gas generator – power turbine engines having only one compressor, the term P_{c2} vanishes.

For journal bearings, as commonly used in industrial scale gas turbines, friction caused by the bearings (torque resisting the rotation) may be assumed proportional to the rotation speed if the viscosity of the lubricating oil and the oil pressure remain unchanged, as according to Moore [1975]. Given by the equation $P=M\omega$, the bearing losses of the gas turbine on operating outside design conditions are thus presumed to be proportional to the square of the rotational speed, as

$$\frac{P_{loss\,j}}{P_{loss\,j0}} = N_{rel\,j}^{2} \tag{4.55}$$

For the sake of universal applicability, the consideration of generator and transmission off-design efficiencies have been omitted providing the feasibility to apply the model to other cases besides electricity production, for example, mechanical energy production. However, the change in efficiencies can be taken into consideration with corresponding efficiency terms for off-design operation.

$$\eta_{gear} = \frac{P_{gear}}{P_{mech}} \tag{4.56}$$

$$\eta_{gen} = \frac{P_{e}}{P_{gear}} \tag{4.57}$$

For electricity production, the speed of the generator shaft is normally maintained at a constant level due to the requirements of the electrical network. Consequently, the influence of the rotational speed on the losses which arise in the transmission and generator is usually neglected – the losses are assumed to vary only with the power transferred. Generally, the variation of relative power losses and corresponding efficiencies over a wide operational range is small.

Denoting the external heat addition to the gas turbine cycle as Φ_{fu}, the thermal efficiency and net efficiency (overall efficiency for electricity production) for the rating of a gas turbine cycle can eventually be determined to be

$$\Phi_{fu} = q_{mfu}\left(q_i + h_{fu}\right) \tag{4.58}$$

$$\eta_{th} = \frac{P_{th}}{\Phi_{fu}} \tag{4.59}$$

$$\eta_e = \frac{P_e}{\Phi_{fu}} \tag{4.60}$$

$$\Rightarrow \quad \eta_e = \eta_{th}\,\eta_{mech}\,\eta_{gear}\,\eta_{gen} \tag{4.61}$$

Some of the energy produced on actual gas turbines will be used for driving diverse auxiliary devices and systems, control and lubrication systems for example. In addition to electric power, mechanical power may be required as well. Though far from insignificant, this auxiliary power is customarily not considered here.

5 MATHEMATICS OF COMPUTATION

Apart from the human nature habitual tendency to preserve conventionality, two practical reasons may be seen to have restrained the use of techniques for solving sets of non-linear equations. One is the required computing capacity, these routines perform calculations with matrices of high dimensions. The other reason arises from the complexity and uncertainty of multidimensional root finding itself. However, with the speed of computation doubling approximately every 18 months, and with the application of mathematical techniques to combine globally robust convergence with a locally fast convergence rate, a vast field of opportunities has emerged, even for personal computers.

Multidimensional root finding provides an efficient alternative to the conventional trial-and-error-based iteration procedures[1] – matching procedures – for the performance prediction of gas turbines. To compare the efforts required in both these methods, Figure 11 demonstrates as an example the computational routines needed for matching the overall operation of a twin-shaft engine with a power turbine, as presented by Cohen et al. [1987]. Using root finding methods, only a set of equations that correspond to the process equations, and mass and energy balances for the basic components need to be determined.

What might here seem as an unjust comparison due to the far more elaborate calculus of the equation solving methods, is nevertheless an inevitable indication of the benefits gained with this approach when applying it to different cycles. Both cases require a similar number of relations for the basis of the solution, but while the conventional methods each time require a new configuration-based algorithm, only one universal method will be needed for the equation solving technique. As a conclusion, this alternative method will not decrease the need for the theoretical knowledge of the process, but it will essentially facilitate the use of this information to obtain the actual results.

[1] Solving non-linear sets of equations invariably proceeds by iterative improvements of the approximative solutions, too. However, in this thesis, *iteration procedure* refers to methods specifically comprising of the consecutive determination of single terms.

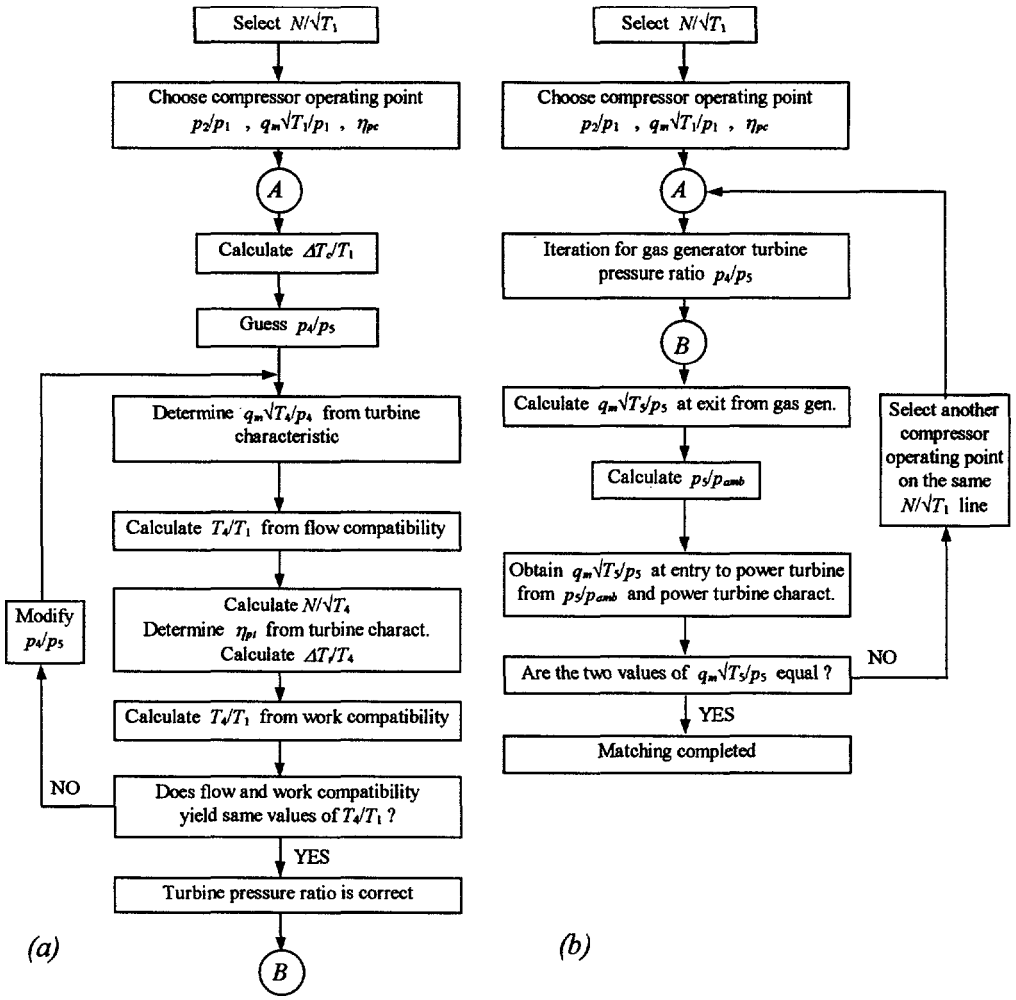

Figure 11. The computational effort for matching the overall operation of a twin-shaft engine with a power turbine as given by Cohen et al. [1987]. *a)* The iteration for the gas generator *b)* the overall iteration procedure.

5.1 Solving the systems of non-linear equations

To exemplify the complexity of finding solutions for a system of non-linear equations, let us consider a case of two dimensions which we want to solve simultaneously

$$\begin{cases} f_1(x_1, x_2) = 0 \\ f_2(x_1, x_2) = 0 \end{cases}$$

The solutions of each of the equations can be plotted as points or zero contour lines on the (x_1,x_2) plane, as demonstrated in Fig. 12. In general, the arbitrary functions f_1 and f_2 are independent of each other, and the number of disjoint curves for each function is unknown. The solutions for the set of equations consist of the points that are common to both these zero contours. For cases with n dimensions, solving the set of equations correspondingly means finding points mutually common to n unrelated zero-contour hypersurfaces, each of dimension n-1.

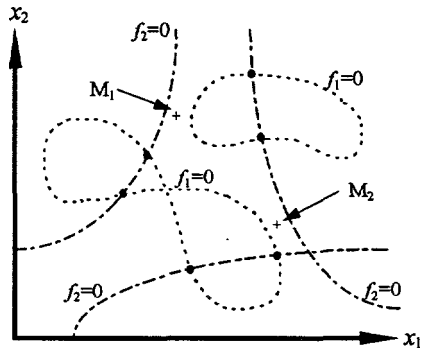

Figure 12. Zero curves of two non-linear functions f_1 and f_2 in two unknowns. The solutions (dots) for the corresponding set of equations may be found from the intersections of these curves.

Without any insight into the problem, finding all common points is obviously impossible, except in theory, by mapping out the full zero-contours of both functions. Consequently, there are no general methods of solving systems of non-linear equations that would converge to a root regardless of the initial guess.

5.1.1 Methods for the solution

There exist some techniques that proceed from a given starting point and (hopefully) find one solution. Most of them use Newton's method as a basis, improving its poor global convergence[1] properties and/or decreasing the need for computation, as described by Dennis et al. [1983], for instance. Another class of algorithms are based on homotopy – or continuation – methods, as by Watson et al. [1987]. These methods define a trivial problem for which the solution is known, and a

[1] A multidimensional root finding method is defined by Dennis et al. [1983] as *globally convergent* if it converges to some solution of a system of non-linear equations from almost any starting point. This is a distinction from *locally convergent* algorithms where it is imperative that the starting point is located in the appropriate neighbourhood of the actual root.

path between this easy problem and the hard problem that is actually of interest. Global optimisation[1], see Törn et al. [1989], for instance, provides yet another set of techniques that has the potential for solving sets of non-linear equations. While global minimisation is the task of finding the absolutely best set of parameters to minimise an objective function, multidimensional root finding converts into a minimisation task by, for instance, summing the squares of the individual co-ordinate functions to get the objective function. This function is nonnegative and has a global minimum at any solution of the non-linear equations.

For this study, Newton-based methods have been chosen for the sake of their prevalence in literature. Newton's method guarantees a fast rate of convergence near the solution. However, in general, it sets too restrictive demands on the accuracy[2] of the starting point for the method to be useful in itself. Partial aid for this poor global convergence can be found from local optimisation. Although multidimensional root finding lacks any general techniques, there are a variety of optimisation methods that converge to a local or global minimum regardless of the starting point, thus being globally convergent. Fundamentally, this arises from the dependencies in the minimisation process: multidimensional root finding corresponds to zeroing an n-dimensional function whereas minimisation is equivalent to finding a zero of an n-dimensional gradient vector, the components of this vector being partly related by differentiation. However, except for the special case of the master function and the feasible region being convex, these local optimisation methods can not be trusted to find the global minimum and therefore they can not be used solely for multidimensional root finding either.

The elementary approach of combining minimisation and root finding techniques for solving sets of non-linear equations uses minimisation only for improving the accuracy of the initial guess (moving the starting point closer to the root), as suggested by Burden et al. [1985], and has proven feasible for the purposes of modelling gas turbine performance, Kaikko [1997]. However, to incorporate global robustness with fast local convergence, more sophisticated strategies usually combine Newton's method with an associated minimisation problem. Consequently, two basic strategies prevail for improving the poor global convergence behaviour of Newton's method, as presented by

---

[1] *Global optimisation* refers to techniques of seeking the absolute minimiser in the existence of many distinct minimisers. This is a distinction from *optimisation* which proceeds by seeking any, local or global minimiser.

[2] The term *accuracy* is used in this context to characterise the distance between the actual point and the solution for the set of equations.

Dennis et al. [1983]: the line search and the model-trust region approach. In the line search strategy, the Newton direction for the step is retained, but the step length is modified to approximately minimise the objective function. For the model-trust region strategy, both the direction and the step length are subject to change. This approach is based on estimating the region in which a local model, underlying Newton's method, can be trusted to adequately represent the function, and taking a step to approximately minimise the model in this region. From these strategies, the former one was chosen for this study.

5.1.2 Typical characteristics of the application of root finding methods

Solving systems of non-linear equations presents a non-linear problem. Typical for these problems is that their deterministic solution proceeds by iterative sequences, thus requiring an initial guess for the starting point. Therefore, on estimating the validity of these methods, not only their computational cost but also their convergence capabilities become significant. Instead of the rate, the domain of convergence of these methods may become decisive here. Furthermore, the performance of the methods can be expected to deteriorate when the dimension of the problem increases, unless the non-linearity is only mild.

Some characteristics when applying root finding methods, especially for the performance prediction of gas turbines, may also be identified. One such characteristic is that the problems are poorly scaled in the sense that the variables vary greatly in magnitude. As an example, efficiencies are normally close to unity, while the values for the pressures (in SI-units) are of the order of hundreds of thousands. In finite-precision arithmetics, this may cause the calculation of the Euclidian norms, for instance, to be undesireably dominated by the greater values and lead to a degradation in performance. Therefore, the variables must be re-scaled before computation to present roughly the same order of magnitude. In this study, the scaling factors for the variables are gained from the initial guess values and retained in an unaltered state throughout the computation. Thus, no dynamic scaling has been implemented.

All the variables and the co-ordinate functions used for this modelling are continuous, but some derivatives of the functions are not. Where continuous derivatives are also required, as for the Jacobian matrix in Newton's method, this can be satisfied by interpolation schemes, for instance. An example of this is given in Chapter 5.3.2.

As a consequence of using functional relationships for dependencies in the model, some derivatives in the Jacobian matrix are difficult to express analytically. Therefore, the Jacobian has been replaced by a finite-difference approximation. Using forward differences, for the *i*th co-ordinate function it may be shown that

$$\frac{\partial f_i(\mathbf{x})}{\partial x_j} \cong \frac{f_i(\mathbf{x}+h\mathbf{e}_j)-f_i(\mathbf{x})}{h} \tag{5.1}$$

In the above formula, h denotes the step size and $\mathbf{e}_j$ the jth unit vector. This approximation formula may be shown to give at best only the square root of the machine accuracy. Therefore, errors that arise in finite-precision computing have been reduced by applying double precision arithmetic for root finding.

The number of variables is typically moderate, say less than 100. Therefore, no techniques for reducing the computational cost, such as secant approximations to replace the Jacobian matrix (or its finite-difference approximation), are required. For the same reason, no sparse matrix techniques have been implemented either, although the co-ordinate functions have typically only few variables and, consequently, most of the derivative terms in the Jacobian are zero.

Due to the physical context of the variables, their order of magnitude can be estimated beforehand, thus facilitating the determination of the the initial guess. Similarly, simple constraints could be set for the variables in the form of upper and lower bounds for facilitating the task of global optimisation. For the Newton-based root finding methods however, these constraints are not taken into consideration.

In general, the number of solutions to the set of equations is unknown. However, for modelling real-world applications like gas turbines, a unique solution can be expected. The existence of unique solutions reflects the steady state operation of the engines: for each operating point there is a unique set of parameters with thermodynamic dependency. If one of the parameters varies independently, the others will vary dependently causing a change in the gas turbine operating point. Thus, at every operating point, each parameter has a unique value.

5.2 The selected strategy

5.2.1 Newton's method with line search

A set of non-linear equations in n dimensions with the convention that the right-hand side of each equation is zero, consists of n non-linear functional relations to be zeroed simultaneously. By presenting these functions in a vector $\mathbf{F}$ and the variables in $\mathbf{x}$, the vector notation for the set of equations becomes

$$\mathbf{F}(\mathbf{x}) = \mathbf{0} \tag{5.2}$$

The expansion of the functions in the neighbourhood of $\mathbf{x}$ in Taylor series can be presented correspondingly in matrix notation as

$$\mathbf{F}(\mathbf{x}+\delta\mathbf{x}) = \mathbf{F}(\mathbf{x})+\mathbf{J}(\mathbf{x})\delta\mathbf{x}+O(\delta\mathbf{x}^2) \tag{5.3}$$

In the above equation, $O(\delta\mathbf{x}^2)$ denotes the terms of order $\delta\mathbf{x}^2$ and higher, $\mathbf{J}(\mathbf{x})$ is the Jacobian matrix at $\mathbf{x}$

$$\mathbf{J}(\mathbf{x}) = \begin{bmatrix} \frac{\partial f_1(\mathbf{x})}{\partial x_1} & \cdots & \frac{\partial f_1(\mathbf{x})}{\partial x_n} \\ \vdots & \ddots & \vdots \\ \frac{\partial f_n(\mathbf{x})}{\partial x_1} & \cdots & \frac{\partial f_n(\mathbf{x})}{\partial x_n} \end{bmatrix} \tag{5.4}$$

By requiring that $\mathbf{F}(\mathbf{x}+\delta\mathbf{x})=\mathbf{0}$ and neglecting the higher order terms in Eq. (5.3), a set of linear equations remains that determines the approximate correction $\delta\mathbf{x}$ to be added to the solution vector to conform to the basic Newton method for solving sets of non-linear equations. The set of equations can be solved easily using *LU*-decomposition, for instance. Thus, for the correction and the iterative sequence the following applies

$$\mathbf{J}(\mathbf{x}^{(k)})\delta\mathbf{x}^{(k)} = -\mathbf{F}(\mathbf{x}^{(k)}) \tag{5.5}$$

$$\mathbf{x}^{(k+1)} = \mathbf{x}^{(k)}+\delta\mathbf{x}^{(k)} \tag{5.6}$$

As given by Dennis et al. [1983], a necessary precondition for this Newton step $\delta\mathbf{x}$ to produce a converging sequence is that the starting point is sufficiently close to the root. Newton's method

also requires the Jacobian matrix to be non-singular and the partial derivatives in the matrix to be continuous, but it provides efficient convergence once being close enough to the root. While the continuity can be normally taken into consideration already during the modelling of the process, as will be exemplified later, the requirements for the accuracy of the starting point are often difficult to match, thus restricting the use of Newton's method. Furthermore, if not singular, the Jacobian matrix may be numerically ill-conditioned so as to make the computation of the step impossible.

Solving the sets of equations corresponds to a minimisation task by forming an objective function f as the sum of the squares of the co-ordinate functions, and minimising it.

$$f(\mathbf{x}) = \frac{1}{2}\left[\mathbf{F}(\mathbf{x})\right]^{\mathrm{T}} \mathbf{F}(\mathbf{x}) \tag{5.7}$$

The Newton step $\delta\mathbf{x}$ can be shown to be a descent direction for f, thus justifying the line search strategy: moving in the Newton direction will initially decrease f and correspondingly take us closer to the solution. A standard practice is to try the full Newton step first and then check that the proposed step reduces f. If necessary, backtracking along the Newton direction is then bound to give an acceptable step with small enough movements. The implementation of the line search strategy for this study is by Press et al. [1992]. It safeguards both against f decreasing too slowly relative to the step length, and against the step lengths being too small relative to the initial rate of decrease of f. The former safeguard is fulfilled by requiring the average rate of decrease of f to be at least some fraction α of the initial rate of decrease $\nabla f^{\mathrm{T}} \delta\mathbf{x}$:

$$f\left(\mathbf{x}^{(k+1)}\right) \leq f\left(\mathbf{x}^{(k)}\right) + \alpha \nabla f^{\mathrm{T}} \left(\mathbf{x}^{(k+1)} - \mathbf{x}^{(k)}\right) \qquad 0 < \alpha < 1 \tag{5.8}$$

A frequently used value for α is 10^{-4}.

To guard against the step lengths being too small, a lower bound is set for the corresponding step coefficient λ. This value is typically set to be 10 % of the previous backtracking result. Furthermore, it can be shown that if the Newton step failed, for small values of α the optimum step length is bounded from above and does not typically exceed 50 % of the previous value.

The strategy for the backtracking routine can be stated as

$$\text{Define} \quad g(\lambda) \equiv f\left(\mathbf{x}^{(k)} + \lambda\,\delta\mathbf{x}^{(k)}\right) \tag{5.9}$$

$$\text{hence} \quad g'(\lambda) = \nabla f^{\mathrm{T}}\delta\mathbf{x}^{(k)} \tag{5.10}$$

On backtracking, $g(\lambda)$ will be modelled with the most current information available to determine the optimum step coefficient λ. For the first backtrack at each iteration, the routine uses $g(0)$ and $g'(0)$ as well as $g(1)$ from the Newton step to model $g(\lambda)$ as a quadratic. On second and subsequent backtracks, $g(\lambda)$ is modelled as a cubic, using the previous and the second most recent values for $g(\lambda)$.

For the iterative sequence, the following applies

$$\mathbf{x}^{(k+1)} = \mathbf{x}^{(k)} - \lambda\left[\mathbf{J}\left(\mathbf{x}^{(k)}\right)\right]^{-1}\mathbf{F}\left(\mathbf{x}^{(k)}\right) \qquad 0 \le \lambda \le 1 \tag{5.11}$$

It must be noted that when using Newton's method as a basis, no strategy can produce globally converging sequences in general; these strategies only increase the domain of convergence of the basic Newton method. As a theoretical maximum of the domain, the region of attraction is the largest set of points such that for any starting point in that domain the infinitely small step steepest descent algorithm[1] will converge to the root. This region can be visualised in the case of two dimensions as a surface where, if water is poured onto that surface, it will reach the minimiser. However, due to the finite step sizes used by the line search, the actual domain of convergence will be reduced. Considerations of the domain in this case are given in the next chapter.

As a conclusion, there are two principal cases when these Newton-based root finding methods can fail. One is when the Jacobian matrix becomes singular or nearly singular and thus the Newton step can not be determined. For this case, Dennis et al. [1983] suggest a modified Newton step as a result of perturbing a model that approximates **F**, rather than perturbing the Jacobian itself. The method involves monitoring the condition number of the Jacobian and uses *QR*-decomposition for solving the linear set of equations that determines the step. However, Press et al. [1992] have expressed their doubts on the method's usefulness outside exactly singular problems, and it has not been implemented here either. The second failure occurs when the starting point lies outside the domain of convergence. The algorithms proceed by seeking any, local or global minimiser to the

[1] In the method of steepest descent, the steps are taken in the steepest downhill direction. This is the negative of the gradient direction, $-\nabla f$.

problem. Therefore, if started close to a local minimiser, the methods may converge to it instead. In Fig. 12, for instance, the zero contours of f_1 and f_2 make a close approach to each other at the points labelled M_1 and M_2, indicating the likelihood of local minima. Nevertheless, monitoring this false convergence is easy by using the sum of squares as the error term. On encountering this local minimum, a simple remedy is to try another starting point, possibly closer to the root. However, this method is trivial since there is no guarantee against converging back to the same or to another local minimiser. Global optimisation, started from this point, could be one solution here.

5.2.2 Local and global convergence characteristics

It can be shown, as by Dennis et al. [1983] for instance, that the basic Newton method is locally quadratically convergent for most problems, if the Jacobian matrix is non-singular. Thus, near the solution $\mathbf{x}^*$, for the vector 2-norm and for some positive constant β it applies that

$$\left\|\mathbf{x}^{(k+1)} - \mathbf{x}^*\right\| \leq \beta \left\|\mathbf{x}^{(k)} - \mathbf{x}^*\right\|^2 \tag{5.12}$$

Computationally, it means approximately that the number of significant digits will double at each iteration near the solution. If the finite-difference step size is chosen properly, the quadratic convergence may be shown to be retained even when using finite-difference approximations with the Jacobian. Furthermore, this fast local convergence will be retained by using the selected strategies too, if the algorithm tries a Newton step first at each iteration.

Due to a large number of co-ordinate functions, the analytical determination of the local, as well as the global, convergence characteristics for the selected strategy has been omitted here. Instead, a statistical examination has been implemented for two of the example cases in Chapter 6 (types CBE and CBEEX) to characterise the global robustness of the selected method for that case. The results presented in Fig. 13 plot the probability of finding the design-point solution again against randomised deviation of the actual root. For the determination of one data point in the figure, the set of equations is solved repeatedly, each time using different random numbers to uniformly deviate the starting point into the neighbourhood of the actual root, until the method fails to converge back. This sequence is then repeated until statistical validity is achieved. Finally, the probability is obtained as a ratio of the mean number of successful trials to the mean total number of trials (= numerator plus 1). As the results show, increasing the complexity of the model will decrease the domain of convergence: for the simpler model, the probability of convergence exceeds

95 % if the deviation remains below 55 %, while for the more complicated configuration the corresponding allowable deviation range becomes 30 %.

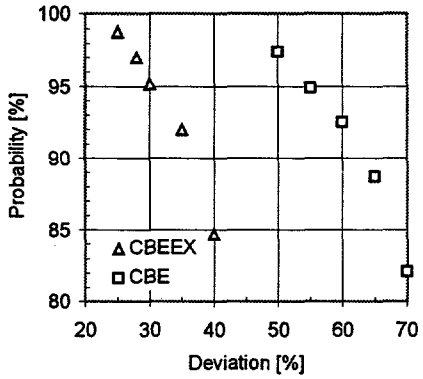

Figure 13. The probability of the selected strategy to produce a converging sequence back to the solution for the design-calculation as a function of a deviation range around the actual root for two example cases in Chapter 6.

It must be noted that the deviation range used in this statistical approach does not in general correspond with the actual domain of convergence for the method, which is due to the asymmetry of the domain. Consequently, a probability of unity would mean in this context only that all the randomly deviated starting points will locate within a subset of the domain of convergence. In directions from the root in which **F** is less non-linear, the region of convergence is likely to be greater. Information that is more specific can be obtained by examining the region of convergence separately in each direction, for instance. However, the bounds that are gained with this study do not define the actual domain of convergence, either, since they show the allowed deviations for the variables only in separate directions.

The elementary way of providing an initial guess is for the user to determine and supply the values. This is, however, a laborious task, especially for a case of high dimensions, so a more sophisticated means of providing the values should be preferred. One method is by the simplification of the calculus routines – to a level where no iterative procedures are required. Major simplifications for the design state calculations for the configurations in this study become as follows:

- Considering the working fluid as air throughout the gas turbine
- Defining the values for specific heat capacities according to the inlet state
- For multi-shaft configurations, assuming the division of the turbine pressure ratios to be equal to the division of the compressor pressure ratios; or assuming the turbine pressure ratios equal if there is only one compressor unit

In this study, an algorithm using the above simplifications produced starting points within the domain of convergence without any exceptions.

For the performance prediction of gas turbines, the problem of supplying an initial guess is only concerned with the design state calculations. The same design model is underlying in the off-design model with additional information serving only to determine the transition from design conditions to off-design. Therefore, if necessary, the path between the conditions can be divided into sub-intervals and the solution proceeds by applying the result of the previous transition as the starting point for the next one. This was, however, not implemented in this study since for all the calculations in Chapter 6, the use of the same algorithm to provide the starting points for the design and off-design calculations proved to be successful.

Since the performance prediction of gas turbines proceeds by always determining the corresponding design values, the method presented in this study is especially suitable for purposes where the reference state is already known and only the deviations from that state need to be determined without having to supply the starting point. This is a typical case for condition monitoring aspects in gas turbines, for instance.

Independent of the cycle configuration, a more universal means of providing starting points could be implemented by global optimisation methods. However, they are not considered in this study.

5.3 Subroutines for the equations

In some cases, the use of algebraic equations for the determination of the relations between variables may not be reasonable due to modularity applied by the computation, or resulting from complex calculation procedures. Subroutines will be used then instead, denoted by $f_1..f_{12}$, for providing values corresponding to specific arguments. This essentially simplifies the formal state of the set of equations, though not complicating the finding of the root provided that the requirement for continuous derivatives will be fulfilled. Thermodynamic properties, component characteristics, and conversion equations between isentropic and polytropic efficiencies, Eqs. (3.31) and (3.32), apply to this method.

5.3.1 Thermodynamic state properties

Determining the operating values for gas turbine cycles is principally founded on the thermodynamic state properties of the working fluid. This fluid may be classified into fuel, air or flue gases from stoichiometric combustion, consequently affecting the determination of the properties – specific heat capacity, enthalpy, specific gas constant, lower heating value for the fuel and the amount of air for stoichiometric combustion. In this study, the computation of the properties utilises polynomial functions for specific heat capacities of gaseous components, a table for combustion reactions, and molecular heating values for these reactions, as presented in Larjola [1990]. The assumption of a perfect gas will provide a basis for the computation, having specific heat capacity as well as enthalpy varying with temperature only.

For the specific heat capacities of the gas components (referred to with a subscript *j*), third degree polynomials will be used which have been attained from tabulated values. Accordingly, the specific heat capacity of the gas mixture (f_1) can be calculated by weighting by the mass fraction of the components as follows

$$c_{pj}(T) = c_{0j} + c_{1j}\,T + c_{2j}\,T^2 + c_{3j}\,T^3 \tag{5.13}$$

$$c_p(T) = c_0 + c_1\,T + c_2\,T^2 + c_3\,T^3 = f_1(fluid, T) \tag{5.14}$$

$$\begin{cases} c_0 = c_0(fluid) = \sum_j \left(y_j\, c_{0j}\right) \\ \vdots \\ c_3 = c_3(fluid) = \sum_j \left(y_j\, c_{3j}\right) \end{cases} \tag{5.15}$$

Occasionally, fits for heat capacity may comprise of additional terms, such as factors inversely proportional to some powers of temperature, as given by Reynolds [1979], for instance. However, for the temperature span typically in the region of 200 to 1800 K in this model, third degree polynomials have been found to provide sufficient accuracy to justify their use.

A presentation for the specific enthalpy of the gas mixture (f_2) can be obtained by integrating the equation $dh = c_p dT$. According to the ISO 2314 standard, the temperature chosen for zero enthalpy is +15 °C, denoted with T_{ref}.

$$\begin{aligned} h(T) &= c_0\left(T - T_{ref}\right) + \frac{1}{2}c_1\left(T - T_{ref}\right)^2 + \frac{1}{3}c_2\left(T - T_{ref}\right)^3 + \frac{1}{4}c_3\left(T - T_{ref}\right)^4 \\ &= f_2(fluid, T) \end{aligned} \quad (5.16)$$

In this model, compositions of air, fuel oil, natural gas and bio gas have been pre-determined. The composition of the stoichiometric combustion gases corresponding to the fuel will be calculated using the combustion reactions. For any other fuels, their composition has to be supplied by the user before computation. For fuel oil, a fit for the specific heat capacity and the lower heating value has been pre-determined too, since they can not be defined on a mere elementary basis that is frequently given for fuel oils.

Corresponding to the specific fuel, the combustion reactions also provide the molal amount of air required for stoichiometric combustion, denoted as N_{sa}/N_{fu}. Employing the molecular mass for the fuel as a sum of component masses weighted by the mole fractions, the specific amount of air for stoichiometric combustion (f_3) then becomes

$$L = \frac{N_{sa}}{N_{fu}} \frac{M_a}{\sum_j \left(x_j M_j\right)} = f_3(fluid) \quad (5.17)$$

The lower heating value of the fuel (f_4) can be calculated using the molecular heating values given for the components as

$$q_i = \frac{\sum_j \left(x_j Q_{mj}\right)}{\sum_j \left(x_j M_j\right)} = f_4(fluid) \quad (5.18)$$

The specific gas constant (f_5) is the ratio of the universal gas constant to the molecular mass of the corresponding fluid. The value for the universal gas constant is $R_u = 8.31434$ J/(mol K).

$$R = \frac{R_u}{\sum_j \left(x_j M_j\right)} = f_5(fluid) \quad (5.19)$$

In addition, the dynamic viscosity of air will be required for determining the operation of the heat regeneration system. A third degree polynomial fit for viscosity (f_6) has been obtained from the tabulated values as a function of temperature, as presented in VDI-Wärmeatlas [1988].

$$\mu_a(T) = c_0 + c_1 T + c_2 T^2 + c_3 T^3 = f_6(T) \tag{5.20}$$

5.3.2 Performance maps

The maps for compressors and turbines present constant parameter curves. Therefore, an inherent way of modelling these maps would consist of approximating these curves with appropriate polynomial fits and using basic bivariate interpolation schemes. For any value of the curve parameter, the surrounding curves on the map would then be transferred to approximate the curve that corresponds to this value, obtaining the result by a linear interpolation of these curves. This kind of interpolation is easy to implement and generally gives good results, as demonstrated by Münzberg et al. [1977], for instance. However, this method does not ensure the continuity of the first derivatives as the interpolating point crosses the approximating curves and therefore it is not suitable here.

In this study, the continuance of the derivatives has been maintained by the use of cubic splines, as implemented by Press et al. [1992]. The cubic spline interpolation uses cubic piecewise polynomials, matches with the data points, and has continuous first and second derivatives. An extension of the method for two variables is the bicubic spline.

According to Chapter 4.1.2, the presentation of the compressor maps is assumed to comprise three variables: Φ, Π, and β. However, this interpolation can be carried out in two stages: first using variables Φ and Π to yield values from the maps presented for various blade settings β, and then using these values for interpolation with the corresponding β.

As a result, subroutines for the interpolation of the compressor mass flow and efficiency (f_9 and f_7) use first bicubic and then cubic splines. A term for the pressure ratio at the surge line is a function of the rotational term and the blade setting, therefore it applies two consecutive cubic spline

interpolations (subroutine f_{10}). The subroutine for the turbine efficiency interpolation (f_8) uses single bicubic spline evaluation only.

$$\frac{\eta_{sc}}{\eta_{sc0}} = f_7\left(\Pi_c, \Phi_c, \beta\right) \tag{5.21}$$

$$\frac{\eta_{st}}{\eta_{st0}} = f_8\left(\Pi_t, \Phi_t\right) \tag{5.22}$$

$$\frac{q_m}{q_{m0}}\sqrt{\frac{T_\alpha}{T_{\alpha 0}}}\frac{p_{\alpha 0}}{p_\alpha} = f_9\left(\Pi_c, \Phi_c, \beta\right) \tag{5.23}$$

$$\Pi_{cs} = f_{10}\left(\Phi_c, \beta\right) \tag{5.24}$$

The bicubic spline interpolation is based on rectangular-grid data[1]. Therefore, for a compressor mass flow map for instance, curves for small values of Φ have to be extended into the surge area to cover the entire variation range for Π. The point of convergence for the curves must be smooth since the splines cannot yield high accuracy near the edges. Except for in the close neighbourhood of the surge line, the shape of the curves in the surge area does not affect the results.

The accuracy of the interpolation is heavily influenced by the density of the data grid. For the compressor map, for instance, satisfactory results were not gained until the number of curves was increased by placing three auxiliary curves between the original ones, and the spacing for the data points along the Π-axis was reduced to 0.05.

To reduce the amount of work in supplying the grid data, the basic bivariate interpolation has been applied to determine mean curves between the curves of $\Phi = 0.7, 0.75, 0.8, 0.85, \ldots$. For efficiency maps, the translation of the surrounding curves follows the line between the maximum efficiency points. For the compressor mass flow map, the translation line is determined by the points of intersection with the surge line. For this bivariate interpolation scheme, values for the surrounding curves have been obtained with cubic splines. For the reduction of the spacing in the Π-axis from 0.1 to 0.05, cubic splines were also implemented.

[1] An algorithm that performs bivariate interpolation and smooth surface fitting for scattered (irregularly distributed) data is presented by Akima [1996]. It is a local, triangle-based algorithm which uses a fifth-degree polynomial for the interpolation.

Curves that are gained with this method, as well as points from the bicubic spline interpolation for the compressor mass flow map is presented in Fig. 14. This figure indicates reasonable validity, both for the added curves and for the interpolation results.

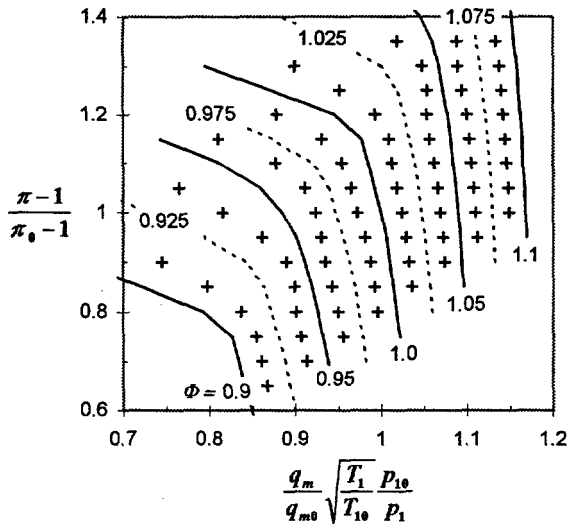

Figure 14. A section of the compressor mass flow map illustrating the original and the auxiliary curves (Φ = 0.9, 0.95, 1.0, 1.05 and 1.1), curves that correspond with the computational determination (Φ = 0.925, 0.975, 1.025 and 1.075), and the results from the bicubic spline interpolation (+ sign) corresponding to the mean value of the surrounding curves.

In general, the pressure ratio for the compressor shows an increasing tendency when mass flow decreases. Consequently, for every set of Π and Φ, there is only one value for mass flow. Occasionally, near the surge line the relationship may turn to show an increasing tendency instead. Although this area cannot be modelled correctly using Π and Φ, it is of no significance to the validity of the model as the steady state operation of the gas turbine is not possible in this unstable zone either.

5.4 The basic set of equations

Resulting from the considerations given in the previous chapters, the modelling of gas turbine performance in this study can be divided into subsystems as shown in Table 1. This basic set of equations will cover a variety of non-reheating gas turbine cycles and is irrespective of the shaft

number. The application of these components for constructing a model for a specific gas turbine configuration incorporates numbering the cycle points – flow-wise, for instance, and setting the mass flows consistent with the flow arrangement.

Design state values provide a basis for evaluating the off-design performance, so they have to be calculated first. Supplementary equations for determining the behaviour outside design state (denoted with an asterisk) will be trivial at this stage and can be neglected. On calculating off-design state values, all equations will apply instead.

Table 1. The equations for modelling gas turbine performance after the division into subsystems. An asterisk refers to equations not applicable for determining the design operation.

a) Inlet ducts

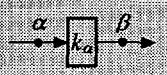	$T_\beta = T_{amb}$
	$h_\beta = f_2(a, T_\beta)$
$p_\beta = (1-k_\alpha)\, p_{amb}$	$*\dfrac{k_\alpha}{k_{\alpha 0}} = \left(\dfrac{q_{m\alpha}}{q_{m\alpha 0}}\right)^2 \left(\dfrac{p_{amb\,0}}{p_{amb}}\right)^2 \dfrac{T_{amb}}{T_{amb\,0}}$

b) i:th compressor, j:th shaft

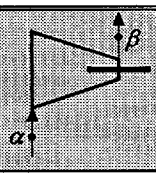	$T_\beta = T_\alpha\, \pi_{ci}^{\frac{R_c}{\bar{c}_{pci}\,\eta_{pci}}}$
	$p_\beta = \pi_{ci}\, p_\alpha$
$P_{ci} = q_{m\alpha}(h_\beta - h_\alpha)$	$\bar{c}_{pci} = f_1(a, \bar{T}_{\alpha,\beta})$
$h_\beta = f_2(a, T_\beta)$	$\eta_{sci} = f_{11}(\eta_{pci}, \pi_{ci}, \bar{c}_{pci}, R_c)$
$*\dfrac{q_{m\alpha}}{q_{m\alpha 0}} = \sqrt{\dfrac{T_{\alpha 0}}{T_\alpha}}\, \dfrac{p_\alpha}{p_{\alpha 0}}\, f_9(\Pi_{ci}, \Phi_{ci}, \beta_i)$	$*\dfrac{\eta_{sci}}{\eta_{sci0}} = f_7(\Pi_{ci}, \Phi_{ci}, \beta_i)$
$*\Pi_{ci} = \dfrac{\pi_{ci}-1}{\pi_{ci0}-1}$	$*\Phi_{ci} = N_{rel\,j}\sqrt{\dfrac{T_{\alpha 0}}{T_\alpha}}$
$*Y_i = \dfrac{\Pi_{csi}(\pi_{ci0}-1)+1-\pi_{ci}}{\pi_{ci}}$	$*\Pi_{csi} = f_{10}(\Phi_{ci}, \beta_i)$

c) Heat exchanger - intercooler

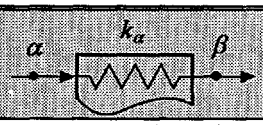	$h_\beta = f_2(a, T_\beta)$
$p_\beta = (1-k_\alpha)\, p_\alpha$	$*\dfrac{k_\alpha}{k_{\alpha 0}} = \left(\dfrac{q_{m\alpha}}{q_{m\alpha 0}}\right)^2 \left(\dfrac{p_{\alpha 0}}{p_\alpha}\right)^2 \dfrac{T_\alpha}{T_{\alpha 0}}$

d) Ramification of the cooling flow q_{mco} from i:th compressor discharge

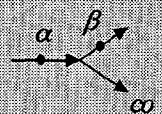	$q_{mco} = y_{co}\, q_{m\alpha}$
	$*\dfrac{y_{co}}{y_{co0}} = \dfrac{p_\alpha}{p_{\alpha 0}} \sqrt{\dfrac{T_{\alpha 0}}{T_\alpha}}\, \dfrac{q_{m\alpha 0}}{q_{m\alpha}}$

e) Heat exchanger - flue gas γ-δ to air α-β

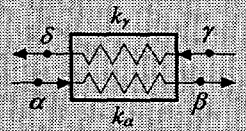	$T_\beta = T_\alpha + \varepsilon(T_\gamma - T_\alpha)$
	$h_\beta = f_2(a, T_\beta)$
	$h_\delta = (1-y)\, f_2(a, T_\delta) + y\, f_2(sg, T_\delta)$
$h_\delta = h_\gamma - \dfrac{q_{m\alpha}}{q_{m\gamma}}(h_\beta - h_\alpha)$	$p_\beta = (1-k_\alpha)\, p_\alpha$
$p_\gamma = \dfrac{p_\delta}{1-k_\gamma}$	$*\dfrac{k_\alpha}{k_{\alpha 0}} = \left(\dfrac{q_{m\alpha}}{q_{m\alpha 0}}\right)^2 \left(\dfrac{p_{\alpha 0}}{p_\alpha}\right)^2 \dfrac{T_\alpha}{T_{\alpha 0}}$
$*\dfrac{k_\gamma}{k_{\gamma 0}} = \left(\dfrac{q_{m\gamma}}{q_{m\gamma 0}}\right)^2 \left(\dfrac{p_{\gamma 0}}{p_\gamma}\right)^2 \dfrac{T_\gamma}{T_{\gamma 0}}$	$*\dfrac{\bar{\mu}_a}{\bar{\mu}_{a0}} = \dfrac{f_6(\bar{T}_{\alpha,\beta})}{f_6(\bar{T}_{\alpha 0,\beta 0})}$
$*\dfrac{\varepsilon}{\varepsilon_0} = \dfrac{q_{m\alpha 0}}{q_{m\alpha}} \dfrac{\bar{\mu}_a}{\bar{\mu}_{a0}} \dfrac{T_\gamma - T_\alpha + T_\delta - T_\beta}{T_{\gamma 0} - T_{\alpha 0} + T_{\delta 0} - T_{\beta 0}} \dfrac{T_{\gamma 0} - T_{\alpha 0}}{T_\gamma - T_\alpha}$	

f) Combustion chamber

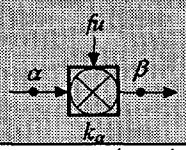	$h_{\beta ISO} = \dfrac{q_{m\alpha}\, h_\alpha + q_{mfu}\left(q_i + h_{fu}\right)}{q_{m\alpha} + q_{mfu}}$
	$h_{6ISO} = (1-y)\, f_2(a, T_{6ISO}) + y\, f_2(sg, T_{6ISO})$
$y_{oc} = \dfrac{(L+1)\, q_{mfu}}{q_{m\alpha} + q_{mfu}}$	$\Phi_{fu} = q_{mfu}\left(q_i + h_{fu}\right)$
$q_i = f_4(fu)$	$h_{fu} = f_2(fu, T_{fu})$
$L = f_3(fu)$	$p_\beta = (1-k_\alpha)\, p_\alpha$
$h_\beta = (1-y_{oc})\, h_{a\beta} + y_{oc}\, h_{sg\beta}$	$h_{a\beta} = f_2(a, T_\beta)$
$h_{sg\beta} = f_2(sg, T_\beta)$	$*\dfrac{k_\alpha}{k_{\alpha 0}} = \left(\dfrac{q_{m\alpha}}{q_{m\alpha 0}}\right)^2 \left(\dfrac{p_{\alpha 0}}{p_\alpha}\right)^2 \dfrac{T_\alpha}{T_{\alpha 0}}$
$q_{mfu} = q_{m\alpha} \dfrac{h_{a\beta} - h_\alpha}{q_i + h_{fu} - (L+1)\, h_{sg\beta} + L\, h_{a\beta}}$	

g) Mixing of the cooled cooling flow q_{mco}

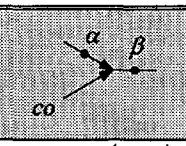	$h_\beta = \dfrac{q_{m\alpha}\, h_\alpha + q_{mco}\, h_{co}}{q_{m\alpha} + q_{mco}}$
$h_\beta = (1-y)\, f_2(a, T_\beta) + y\, f_2(sg, T_\beta)$	$p_\beta = p_\alpha$
$h_\gamma = f_2(a, T_{co})$	$y = \dfrac{(L+1)\, q_{mfu}}{q_{m\alpha} + q_{mco}}$

h) i:th turbine, j:th shaft

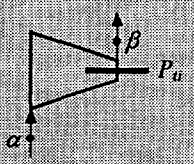	$T_\beta = T_\alpha \, \pi_{ti}^{-\frac{R_t \eta_{pti}}{\bar{c}_{pti}}}$
	$\pi_{ti} = \frac{p_\alpha}{p_\beta}$
$P_{ti} = q_{m\alpha}\left(h_\alpha - h_\beta\right)$	$h_\beta = \left(1-y\right) f_2\left(a, T_\beta\right) + y \, f_2\left(sg, T_\beta\right)$
$\bar{c}_{pti} = \left(1-y\right) f_1\left(a, \bar{T}_{\alpha,\beta}\right) + y \, f_1\left(sg, \bar{T}_{\alpha,\beta}\right)$	$\eta_{sti} = f_{12}\left(\eta_{pti}, \pi_{ti}, \bar{c}_{pti}, R_t\right)$
$*\frac{\eta_{sti}}{\eta_{sti0}} = f_8\left(\Pi_{ti}, \Phi_{ti}\right)$	$*\Pi_{ti} = \frac{\pi_{ti}-1}{\pi_{ti0}-1}$
$*\Phi_{ti} = N_{rel\,j}\sqrt{\frac{T_{\alpha 0}}{T_\alpha}}$	$*\frac{q_{m\alpha}}{q_{m\alpha 0}} = \frac{p_\alpha}{p_{\alpha 0}}\sqrt{\frac{T_{\alpha 0}}{T_\alpha}}\sqrt{\frac{1-\left(\frac{p_\beta}{p_\alpha}\right)^{\frac{2.3}{1.3}}}{1-\left(\frac{p_{\beta 0}}{p_{\alpha 0}}\right)^{\frac{2.3}{1.3}}}}$

i) Outlet ducts

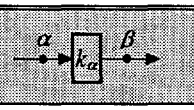	$p_\alpha = \frac{p_{amb}}{\left(1-k_\alpha\right)}$
$T_\beta = T_\alpha$	$*\frac{k_\alpha}{k_{\alpha 0}} = \left(\frac{q_{m\alpha}}{q_{m\alpha 0}}\right)^2 \left(\frac{p_{\alpha 0}}{p_\alpha}\right)^2 \frac{T_\alpha}{T_{\alpha 0}}$

j) Mechanic losses - first shaft, j = 1

$P_{loss1} = \left(1-\eta_{mech}\right) P_{th} - \sum_{i\geq 2} P_{lossi}$	$*\frac{\eta_{mech}}{\eta_{mech0}} = \frac{P_{mech}}{P_{mech0}} \frac{P_{th0}}{P_{mech} + \sum_i \left(P_{lossi0} N_{rel\,i}^2\right)}$

k) Mechanic losses - next shafts, j ≥ 2

$z_j = \frac{P_{loss\,j}}{\sum_i P_{lossi}}$	$*\frac{z_j}{z_{j0}} = \frac{\sum_i P_{lossi0} \, N_{rel\,j}^2}{\sum_i \left(P_{lossi0} N_{rel\,i}^2\right)}$

l) General

$R_c = f_5(a)$	$R_t = (1-y) f_5(a) + y f_5(sg)$
$P_{th} = \sum_i P_{ti} - \sum_i P_{ci}$	$P_{mech} = P_{th} - \sum_j P_{loss\,j}$
$P_e = \eta_{gear}\, \eta_{gen}\, P_{mech}$	$\eta_{th} = \frac{P_{th}}{\Phi_{fu}}$
$\eta_e = \eta_{th}\, \eta_{mech}\, \eta_{gear}\, \eta_{gen}$	$q_{mcg} = q_{ma} + q_{mfu}$
$P_{tj} = P_{cj} + P_{loss\,j}$	*for units with no load only*

Based on the theory employed in this study, there are some limitations for applying the component equations shown above. This model does not include consideration of mixing steam or water with air or combustion gases to improve the performance of stationary gas turbine cycles, such as STIG, ISTIG, RWI or HAT cycles. The prediction of NO_x formation, the by-pass of compressor stages through blow-out valves, and dynamic issues such as transient behaviour are also subjects outside the scope of this study.

The number of the above equations could be significantly reduced by conjoining them whenever possible. Although reducing the size of the matrices for computation, this would correspondingly increase the non-linearity of the system, thus lessen the gains obtained so. Therefore, the equations have been presented and applied at the elementary level.

For twin shaft configurations, the representation of mechanic losses would be simplified by employing a term for the ratio of the mechanic losses as $z = P_{loss1}/P_{loss2}$. The variation of the term would then become $z/z_0 = \left(N_{rel1}/N_{rel2}\right)^2$. Though somewhat more complicated, the formula given in Table 1 is nevertheless universal and extends the coverage to gas turbines with, for instance, three shafts as well. Variation of the mechanic losses outside design operation $\left(P_{loss} \propto N^2\right)$ has been included in the determination of mechanic efficiency and the distribution of the losses.

Table 2 shows one set of fixed values, independent of each other, that are typically used for determining gas turbine performance. Demonstrations in this study will also apply this set of values. Instead of the compressor intake air flow, having the net power as a calculus criteria could

sometimes be reasonable when considering the design operation for instance. Power from the gas turbines is elementarily controlled by affecting the fuel flow, thus outside design conditions, the turbine inlet temperature could be substituted by fuel flow, or again, by net power as a criterion. The computation method demonstrated in this thesis will not be affected by any changes of this kind as long as the fixed values are not interdependent. The routines for supplying the starting point for design state calculations will be affected however.

Table 2. A typical set of fixed values for determination of gas turbine performance.

Design state		Off-design state
Cycle configuration	Turbine cooling rate and temp.	Ambient conditions
Turbine inlet temperature	Intercooling temperature	Turbine inlet temperature
Compressor pressure ratios	Compressor efficiencies	Inlet guide vane settings
Compressor intake mass flow	Turbine efficiencies	Rotational speed for the load
Ambient conditions	Mech. efficiency and distribution	Fuel specifications
Fuel specifications	Gearbox and gen. efficiencies	Turb. cooling and intercooling temp.
Heat exchanger effectiveness	Pressure losses	Gearbox and gen. efficiencies

6 CASE RESULTS

6.1 General

Solving the set of equations for determining the operation of a gas turbine provides temperature, pressure, and enthalpy values for different locations of the cycle, as well as the performance characterising mass flows, power ratings, and cycle efficiencies, for instance. Outside design conditions, the distance of the operating point from the surge line on the compressor map is of interest and will be determined as well. From the computational point of view, the curves for the rotation term in these maps have to be extrapolated into the surge area, and the solution may be found here also. In practice however, the compressor flow has been choked and no static equilibrium state can be presented for the gas turbine. Although printing these values for analysis purposes, a negative surge margin will indicate their imaginary status. In the following off-design considerations, only actual state values have been presented.

The computational time for the models presented in this study was typically in the range of from 1 to 3 seconds when using a PC with a Pentium processor. Thus, for moderate dimensions the elapsed time is not a limiting factor unless real-time simulation is required. In theory, the amount of computation depends on the desired accuracy. For Newton-based methods however, this dependence has a minor role due to the efficient convergence near the root. Nevertheless, the accuracy must be consistent with the internal (machine) accuracy of the numbers, and with the accuracy rendered possible by the approximate derivatives, so that the algorithm will not start reiterating without converging any closer to the root.

Root finding in multidimensions corresponds to zeroing co-ordinate functions. Therefore, the mathematical accuracy of the (inevitably approximative) solution can be easily controlled with the use of the sum of squares of these functions as an error term, the zero value consequently indicating the exact solution. Of course, the correspondence of the results with the real-world performance values depends not only on the mathematical accuracy, but also on the validity of the model itself.

The computer codes for this study use FORTRAN 77 programming language, the interface of the programs being based on a DOS operating system. Although the prevailing Windows environment of today with its graphic interface would certainly provide more convenience to the user, the

character-based DOS system will meet very well the demonstrative needs of this thesis, and has therefore been chosen. Basic versions of the programs perform one design state calculation and another outside design conditions. Other versions comprise a set of design state computations, and a set of determinations for the performance values outside design conditions (in addition with computing the design state values for the off-design case). The output printing of the programs incorporates all the major parameters – the fixed values as well as the results – necessary for viewing the operation of the gas turbines, see Fig. 15 for an example. It must be noted that though the input and output of these programs has been tailored for a specific gas turbine configuration, the computing algorithm for solving the sets of equations is universal.

```
                          GAS TURBINE PERFORMANCE
                             - SI-units -

DESIGN STATE for          Twin shaft engine  -  gas generator and power turbine

Ambient conditions        Tamb 288.15 K     pamb 101.3 kPa     humidity      - %
ISO-turbine inlet temp    1452.3 K          Heat exchanger effectiveness    .900
Fuel  Natural gas         qi 49.06 MJ/kg    Tfu 288.1 K        L 16.87    y .246

Cycle points (K,kPa,kJ/kg)
          1       2       3       4      4M       5       6       7
  T   288.1   536.6   920.8  1500.0  1423.0  1216.3   963.5   634.3
  p   100.3   702.0   688.0   667.3   667.3   311.1   104.4   102.3
  h    15.0   268.8   683.6  1414.7  1312.9  1056.5   754.1   381.8

Power      Pfu      Pc     Pt1     Pt2     Pth   Ploss1  Ploss2   Pmech    Pnet
(MW)    68.497  25.377  26.003  30.659  31.285    .626    .626  30.033  28.231

Mass rate          qma    qmfu    qmcg        qmco/Tco   Cycle     eth    enet
(kg/s)          100.00   1.395  101.40   9.00/536.6 K   eff     .4567   .4121

Component          epc     esc    ept1    est1    ept2    est2   emech     etr
efficiency       .8800   .8447   .8800   .8892   .8800   .8935   .9600   .9400

Pressure         Compr   Turb1   Turb2      k0      k2      k3      k6      k7
ratio and loss    7.00    2.14    2.98    .010    .020    .030    .020    .010

                                                                 Error  .5E-15
-------------------------------------------------------------------------------

OFF-DESIGN STATE          Compressor IGV set at    -  %       Surge margin .215

Ambient conditions        Tamb 278.15 K     pamb  98.0 kPa    humidity      - %
ISO-turbine inlet temp    1356.8 K          Heat exchanger effectiveness    .910
Rotation speed            1st shaft    .957                   2nd shaft     .900
Fuel  Biogas              qi 20.24 MJ/kg    Tfu 293.1 K        L  6.97    y .243

Cycle points (K,kPa,kJ/kg)
          1       2       3       4      4M       5       6       7
  T   278.1   511.7   871.2  1400.0  1329.5  1136.1   906.8   603.1
  p    97.1   650.1   637.3   618.7   618.7   289.7   100.8    98.9
  h     5.0   242.9   628.4  1285.2  1193.6   957.1   686.5   346.6

Power      Pfu      Pc     Pt1     Pt2     Pth   Ploss1  Ploss2   Pmech    Pnet
(MW)    60.049  22.396  22.969  26.283  26.856    .573    .507  25.776  23.714

Mass rate          qma    qmfu    qmcg        qmco/Tco   Cycle     eth    enet
(kg/s)           94.16   2.962   97.12    8.54/511.7 K   eff     .4472   .3949

Component          epc     esc    ept1    est1    ept2    est2   emech     etr
efficiency       .8796   .8449   .8796   .8888   .8749   .8885   .9598   .9200

Pressure         Compr   Turb1   Turb2      k0      k2      k3      k6      k7
ratio and loss    6.70    2.14    2.87    .009    .020    .029    .019    .009

                                                                 Error  .3E-15
```

Figure 15. Example results for twin shaft gas turbines with a gas generator and a power turbine illustrating the output format.

6.2 Example cases

The further examination of solving non-linear sets of equations in this study focuses on three gas turbine configurations as described in Chapter 2.2 – single shaft gas turbines, twin shaft gas turbines comprising a gas generator and a power turbine, and twin shaft intercooled gas turbines with detached low and high pressure units. All the configurations may incorporate heat regeneration. Table 3 shows the composition and sequence of the subsystems for constructing the sets of equations for these cases. Abbreviations for the configurations conform with the main processes - Compression, Burning, Expansion, heat eXchange and Intercooling.

Since the contingency of heat regeneration is taken into account in the models, the effectiveness of the heat exchanger and corresponding pressure losses must be set equal zero if neglecting this process.

Table 3. Composition and sequence of the subsystems for modelling gas turbine configurations with optional heat regeneration. *a)* Single shaft gas turbines (types CBE and CBEX) *b)* twin shaft gas turbines with a gas generator and a power turbine (CBEE and CBEEX) *c)* twin shaft intercooled gas turbines with low and high pressure units, generator on the high pressure shaft (CICBEE and CICBEEX).

a)

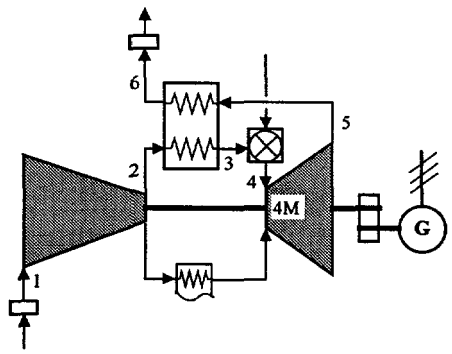

Inlet state	Component Description	Inlet mass flow
ambient	inlet ducts	
1	Compressor	q_{ma}
2	ramification of q_{mco}	
2	heat exchanger / air	q_{ma}- q_{mco}
3	combustion chamber	
4	re-mixing of q_{mco}	q_{ma}- q_{mco}+q_{mfu}
4M	Turbine	
5	heat exchanger / flue gas	q_{mcg}
6	outlet ducts	

b)

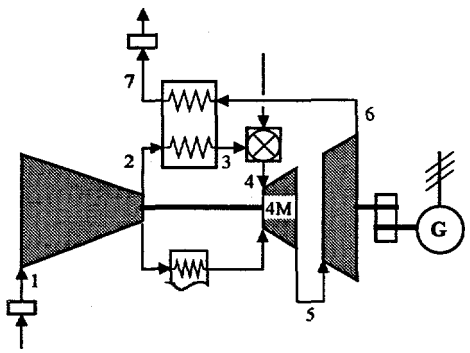

Inlet state	Component description	Inlet mass flow
ambient	inlet ducts	q_{ma}
1	compressor, 1st shaft	
2	ramification of q_{mco}	
2	heat exchanger / air	q_{ma}- q_{mco}
3	combustion chamber	
4	re-mixing of q_{mco}	q_{ma}- q_{mco}+q_{mfu}
4M	1st turbine, 1st shaft	q_{mcg}
5	2nd turbine, 2nd shaft	
6	heat exchanger / flue gas	
7	outlet ducts	

c)

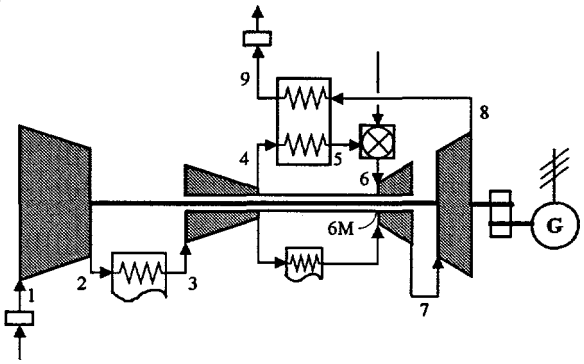

Inlet state	Component description	Inlet mass flow	Inlet state	Component description	Inlet mass flow
ambient	inlet ducts	q_{ma}	5	combustion chamber	q_{ma}- q_{mco}
1	1st compressor, 1st shaft		6	re-mixing of q_{mco}	q_{ma}- q_{mco}+q_{mfu}
2	intercooler		6M	1st turbine, 2nd shaft	q_{mcg}
3	2nd compressor, 2nd shaft		7	2nd turbine, 1st shaft	
4	ramification of q_{mco}		8	heat exchanger / flue gas	
4	heat exchanger / air	q_{ma}- q_{mco}	9	outlet ducts	

The fixed values as applied to all the cases in this study are presented in Table 4. These values provide a basis for examining the influence of the selected turbine inlet temperature, pressure ratio and the degree of heat regeneration on the design power and efficiency rate for the gas turbine

configurations. By setting these values too, the design state performance can be evaluated for the configurations, now providing a basis for off-design calculations.

Table 4. Parameters for examining the influence of turbine inlet temperature, pressure ratio and heat exchanger effectiveness on gas turbine design performance, and as the basis for this case study.

Ambient conditions 15 °C 101.3 kPa 0 %	Intercooling temperature level 50 °C	Relative pressure losses for:
Compressor intake mass flow 100 kg/s	Compressor polytropic efficiencies 0.88	Ducts (inlet , outlet) 0.01 0.01
Fuel specifications Natural gas 15 °C	Turbine polytropic efficiencies 0.88	Combustion chamber 0.03
Turbine cooling rate 0.09	Mechanic efficiency and distribution 0.96 equal	Heat exchanger (air , flue gas) 0.02 0.02
Cooling air temperature level uncooled	Gearbox and generator efficiencies total of 0.94	Intercooler (air side) 0.02

Deviating from the table, some generalisations are worth noting. Each compressor and turbine unit could be configured with a specific efficiency, intermixing polytropic and isentropic efficiencies. Only the properties of the common fuels – fuel oil, natural gas and average bio gas have been pre-determined. Therefore, applying other than these fuels will require determining the specific composition, either in mass or volume fractions, however, still taking into account the limitations described in Chapter 5.3.1.

6.3 Parametric study

6.3.1 Pressure ratio and turbine inlet temperature effect on design operation

The turbine inlet temperature and pressure ratio has a crucial impact on the operation of gas turbines. Figure 16 shows the dependence of design thermal efficiency and specific power (thermal power divided by compressor mass rate) on pressure ratio with different values of actual turbine inlet temperature for single shaft gas turbines without a heat exchanger. The influence of heat regeneration for the same cycle with a turbine inlet temperature of 1500 K can be seen from Fig.

17. These figures along with the others presented in this section are based on results given by the implementation of the case models.

Considering the design operation of gas turbines, the mere division of the compression and expansion processes into smaller units does not affect the process cycle itself. Therefore, with no intercooling (or reheating) introduced, the number of shafts has little influence on the design performance values – primarily, small differences are due to non-uniform combustion and expansion processes. Both the turbines in this study have equal design efficiencies of the polytropic type, which is independent of the pressure ratio, thus Figs. 16 and 17 apply well for twin shaft gas turbines with a gas generator and a power turbine, too. This has been established by the computational results.

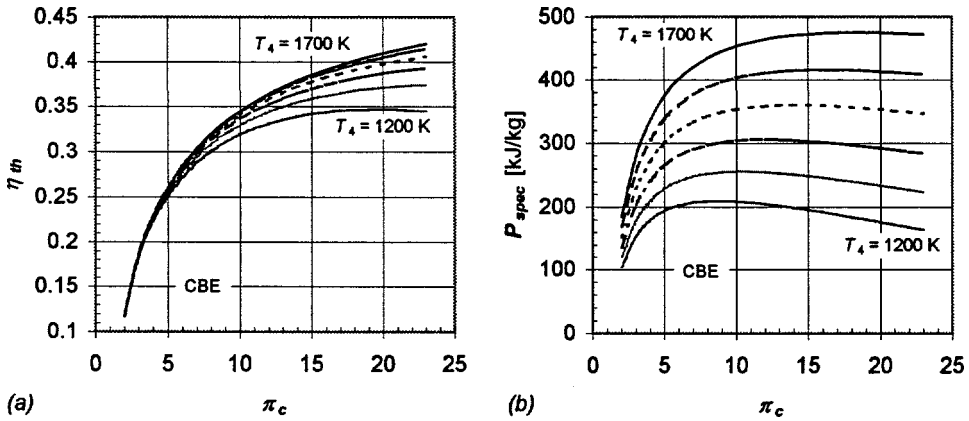

Figure 16. The influence of pressure ratio and actual turbine inlet temperature on design thermal efficiency and specific power for non-regenerating single shaft gas turbines with realistic operating values. The turbine inlet temperature varies in the range 1200 – 1700 K, with 100 degree increments. These curves also apply for twin shaft gas turbines with detached power turbines.

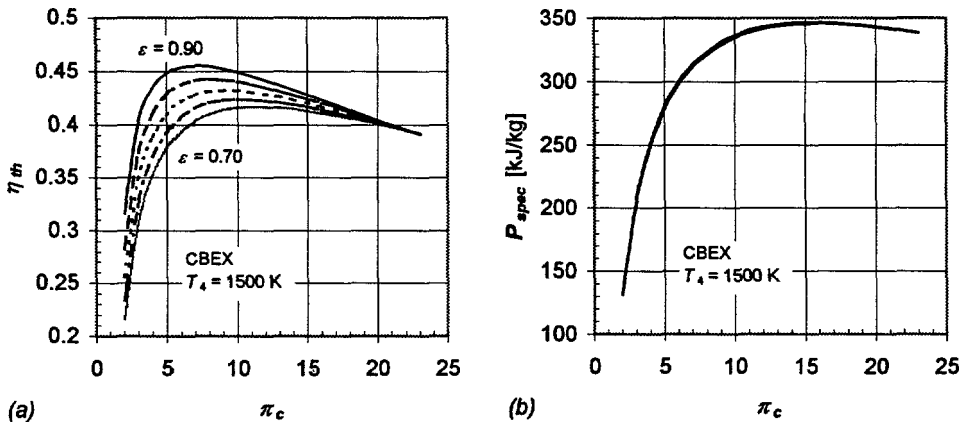

Figure 17. The influence of pressure ratio and heat regeneration on design thermal efficiency and specific power for single shaft gas turbines with a turbine inlet temperature of 1500 K. Heat exchanger effectiveness varies in the range 0.70 – 0.90, with 0.05 increments. These curves apply for twin shaft gas turbines with detached power turbines as well.

According to the figures shown above, without heat regeneration the optimum pressure ratio for thermal efficiency and the pressure ratio to yield maximum specific power both show an increasing tendency with increasing turbine inlet temperature, however they differ from each other. With a constant inlet temperature, increasing the degree of regeneration will decrease the optimum pressure ratio for efficiency, whereas the pressure ratio for maximum specific power remains constant, in this case at a value of approximately 16. Since the gain in efficiency due to regeneration is significant with substantially lower pressure ratios, optimising the efficiency of regenerative gas turbines unavoidably means compromising the specific power, thus increasing the size of the engines. However, for stationary service, engine size seldom has any major role. Therefore, in this study the design values for pressure ratio have been determined by the optimum efficiency alone. The optimum pressure ratio for respective non-regenerative configurations – especially having turbine inlet temperatures at an advanced level – would be considerably high, incorporating, in practice constructional limitations for selecting the pressure ratio. For the demonstrative scope of this study, and for assessing the influence of heat regeneration, all cases will nevertheless apply the pressure ratios optimised by the regenerative cycles. With a selected turbine inlet temperature of 1500 K and a heat exchanger effectiveness of 0.90, the corresponding value for pressure ratio was chosen to be 7, both for single shaft gas turbines and for twin shaft gas turbines with a gas generator and a power turbine.

Figures 18 and 19 show corresponding curves for the intercooled case with the design pressure ratio equally distributed between the compressor stages. Comparing the results of non-regenerative configurations (Figs. 16 and 18), the introduction of intercooling may be seen to provide little or no gain in efficiency, but a remarkable increase in power. Considering the regenerative cycles (Figs. 17 and 19), intercooling will increase the pressure ratio for optimum efficiency, thereby further improving efficiency and power. For twin shaft gas turbines with intercooling and with detached low and high pressure units, the optimum pressure ratio hence becomes approximately 12.

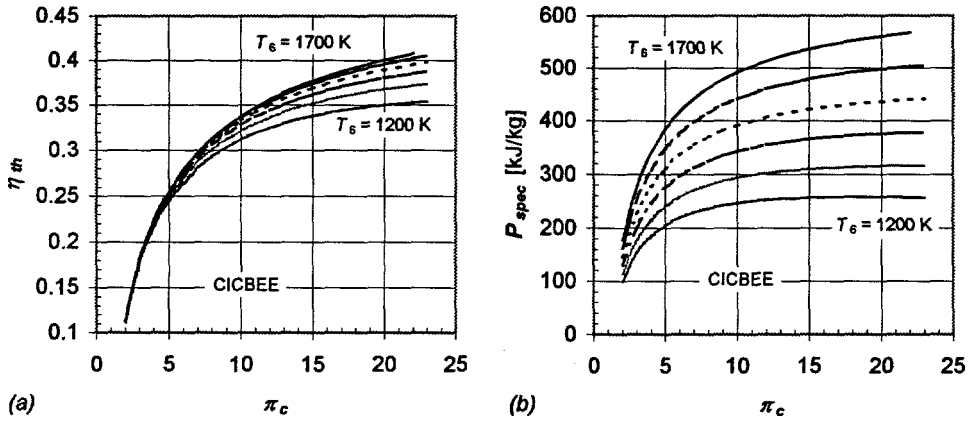

Figure 18. The influence of pressure ratio and actual turbine inlet temperature on design thermal efficiency and specific power for non-regenerative twin shaft gas turbines with detached low and high pressure units. The turbine inlet temperature varies in the range 1200 – 1700 K, with 100 degree increments.

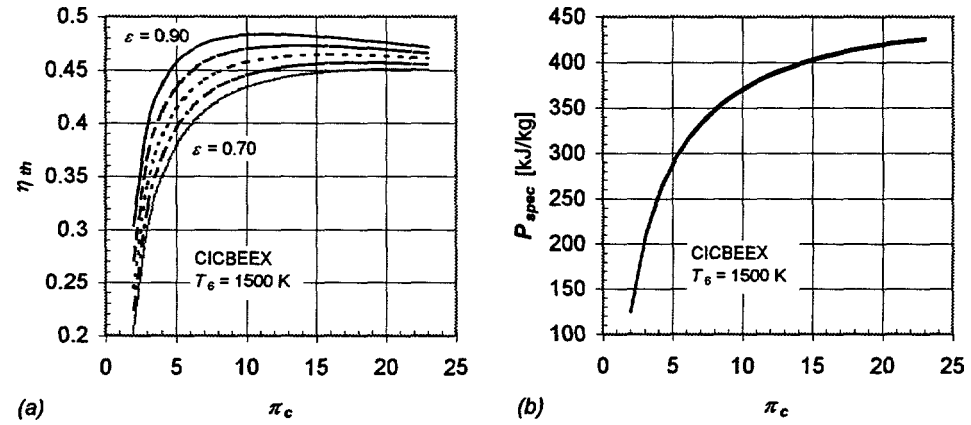

Figure 19. The influence of pressure ratio and heat regeneration on design thermal efficiency and specific power for twin shaft gas turbines with detached low and high pressure units. The turbine inlet temperature is 1500 K, and the heat exchanger effectiveness varies in the range 0.70 – 0.90, with 0.05 increments.

To summarise these constitutive design parameters for the off-design study, the turbine inlet temperature is selected to be 1500 K and the heat exchanger effectiveness for regenerating cycles to be 0.90. Design pressure ratios for the configurations correspond with the optimum efficiency values for the selected degree of regeneration: 7 for single shaft gas turbines (types CBE and CBEX) and for twin shaft engines with detached power turbines (CBEE and CBEEX), and 12 for twin shaft intercooled gas turbines (CICBEE and CICBEEX). The other values used are as in Table 4. The net efficiency and net power rate characterising the design performance of the configurations with these operating values have been presented in Table 5. As the figures show, connecting heat regeneration optimally to a gas turbine cycle will cause only a moderate decrease in power, but a substantial increase in efficiency.

Table 5. Net efficiency and net power rate characterising the design performance of the configurations, and for the reference values outside design conditions.

	CBE	CBEX	CBEE	CBEEX	CICBEE	CICBEEX
η_{e0}	0.272	0.411	0.273	0.412	0.316	0.437
P_{e0} [MW]	30.0	28.1	30.2	28.2	36.7	34.7

6.3.2 Off-design phenomena

To outline the behaviour of the example cases outside design conditions, it is most convenient to examine the effect of the values from Table 2 being altered individually. Based on the results obtained from the model, Figures 20 to 23 present the influence of ambient pressure and temperature, turbine inlet temperature and the rotational speed of the load on the net efficiency and net power rate for the first two configurations. All the computations in this chapter apply the same compressor map as presented in Fig. 5, and the turbine efficiency map of Fig. 8. No variations in the compressor geometry are assumed.

Although the curves that are presented here will strictly apply for these example cases only, the trends in the figures may be considered somewhat characteristic of the specific configurations. In general, variations in the curves for different engines are mainly caused by varying operating values and differing compressor and turbine maps, especially if the nominal operating point is not congruent with the optimum efficiency, as has been the case in this study.

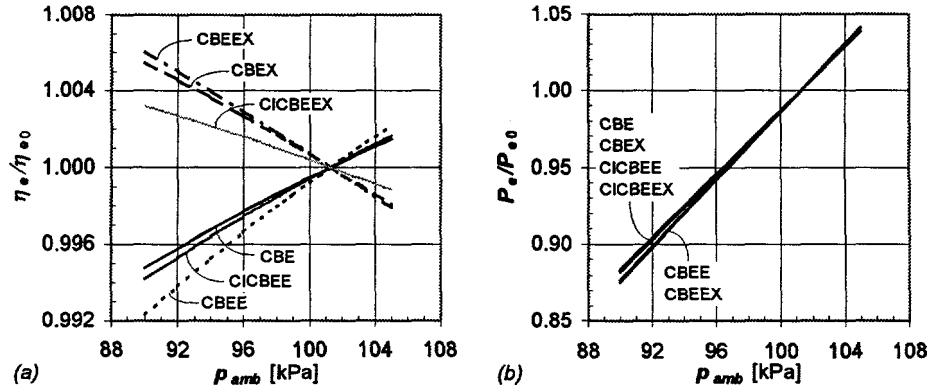

Figure 20. The influence of ambient pressure on net efficiency and net power for the example cases.

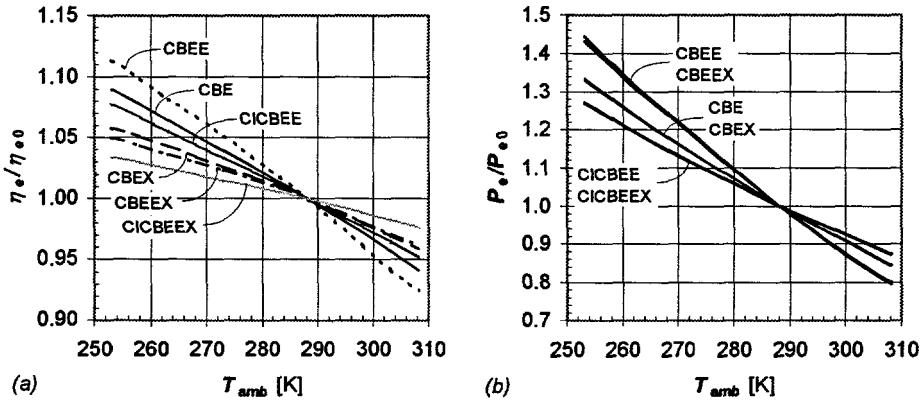

Figure 21. The influence of ambient temperature on net efficiency and net power for the example cases.

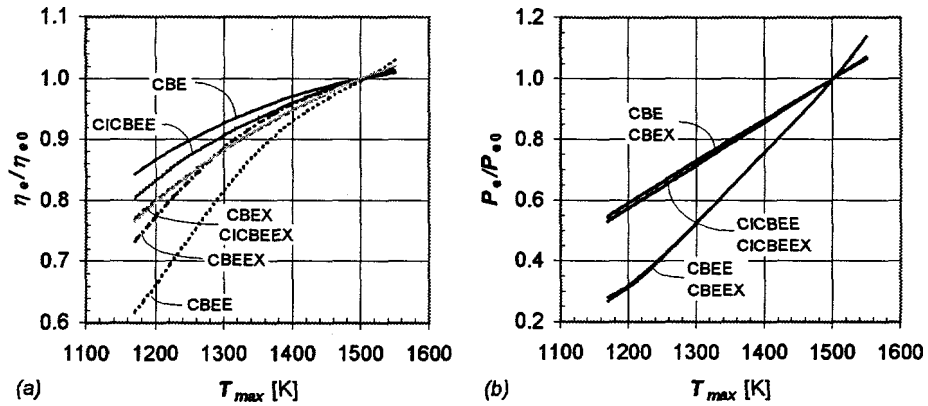

Figure 22. The influence of turbine inlet temperature on net efficiency and net power for the example cases.

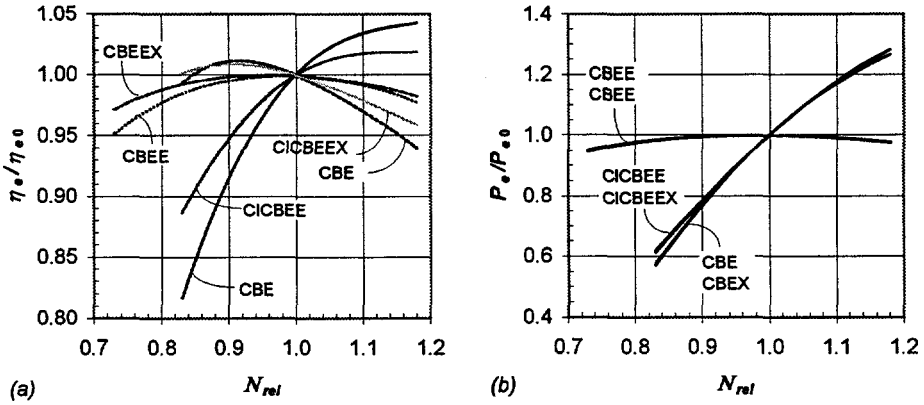

Figure 23. The influence of rotational speed of the load on net efficiency and net power for the example cases.

As can be seen from the figures, the main differences between the cycles arise from the influence of turbine inlet temperature and rotational speed of the load. The expected ranges for the part-load, as well as for the speed of rotation, show considerable advantages for the twin-shaft configurations. Outside the design operation, heat regeneration only effects a variation in the efficiency, not in the power output.

In practice, the differing influence of the turbine inlet temperature for the regenerating cycles can be seen in the part-load efficiencies, as presented in Fig. 24. For constant speed operation, as is the case here, control of the power by the turbine inlet temperature has a much smaller effect on the part-load efficiency for the twin-shaft cycle. However, if the performance of the gas turbines is assumed to follow, for example, the well known propeller-law, as $P \sim N^3$, the part-load efficiency behaviour will change drastically: at 60 % part-load, the efficiency of the single shaft configuration will increase from 80.5 % to 98.8 % of its design value. For the twin-shaft configuration, the corresponding efficiency rise is only from 91.5 % to 92.7 %.

Figure 25 presents the difference in the net torque (given by $P_e = M_e \omega$) between the configurations, as a result of the individual alteration of the rotational speed. Deviating from the single shaft configurations, the torque of the twin shaft configurations will increase with a decrease in the rotational speed, thus making it less sensitive to the load.

Many applications require that the load and the rotational speed can alter independently. As an example, Figure 26 presents the variation of the efficiency under these conditions for the twin-shaft configuration with regeneration. The power is controlled by the turbine inlet temperature. In this case too, the rotational speed for the optimum efficiency shows a decreasing tendency with decreasing power.

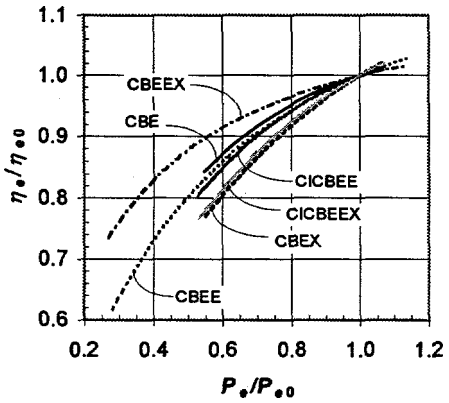

Figure 24. Net efficiency during part-load operation with constant speed; turbine inlet temperature as power control.

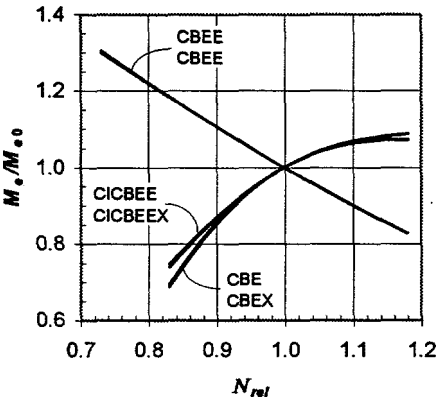

Figure 25. The influence of rotational speed on net torque for the example cases.

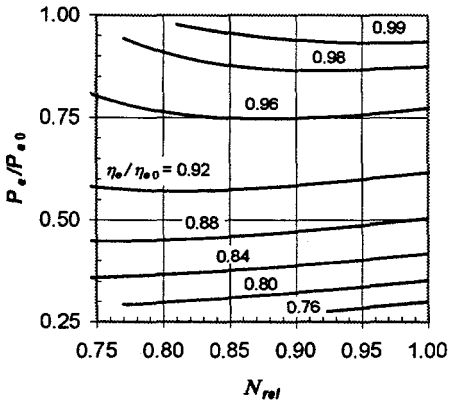

Figure 26. Constant efficiency curves for twin shaft gas turbines with heat regeneration.

If the operating parameters for the gas turbines show only a minor deviation from their design values, the overall effect of the variations on the performance values can be approximated as a multiplication of the individual effects. As a consequence, the curves shown in Figs. 20 to 23 are frequently used for predicting the performance of actual gas turbine engines – for the correction of

the performance values to correspond with the ISO-conditions, for instance. In practice however, the effects of the varying parameters are influenced by each other, thus making this kind of evaluation only valid close to the design conditions. With this method for instance, with decrease of 5 % on the values of the ambient conditions, the turbine inlet temperature and the rotational speed for the example case will inflict a relative error of 1.9 % on the power rating of the regenerative twin-shaft gas turbines with power turbines. Doubling the decrease of the operating parameters will more than triplicate the error.

6.4 Validation studies

In the previous chapter, the effects of some modelling parameters on the performance of gas turbines was considered for the example cases (Figs. 16 to 23). This sensitivity analysis can be applied, for instance, to estimate the influence of erroneous measurement data. To examine the validity of the model, the effect of the perturbations on the model will be considered next. Hereby, the influence of the erroneous component characteristics on the performance values can be estimated. Comparative results from some actual gas turbines and this model will also be given. In this chapter, the study focuses on single shaft engines.

6.4.1 The influence of component characteristics

To explain the role of compressor and turbine characteristics on the performance of gas turbines, let us consider the determination of the operating point for a single shaft engine. The interaction of the compressor and the turbine dictates the gas turbine performance outside design conditions: the pressure ratio and mass flow for the turbine have to correspond with the compressor discharge. With minor simplifications (equal compressor and turbine mass flows, constant pressure losses), the ellipse law for the turbine mass flow can be presented analytically along with the compressor map from Fig. 5 for instance, the curve parameter for the turbine being the temperature ratio T_4/T_1. The intersection of the compressor and turbine curves will determine the operating point for the gas turbine, and the movement of the point can be examined with respect to changes in the modelling parameters. Taking into consideration the proximity of the operating points to the compressor surge line, the widest possible operating range can also be evaluated.

Based on results given by the model, Fig. 27 shows the corresponding range of possible operating conditions for the example case CBE. As can be seen from the figure, for a compressor which is interlinked with a turbine, the range is considerably reduced. Increasing turbine inlet temperature and, consequently, power takes the operating point closer to the surge line whereas an increase in ambient temperature normally affects to the contrary. The influence of the individual increase of the parameters p_{amb}, T_{amb}, T_4 and N_{rel} is presented in Table 6.

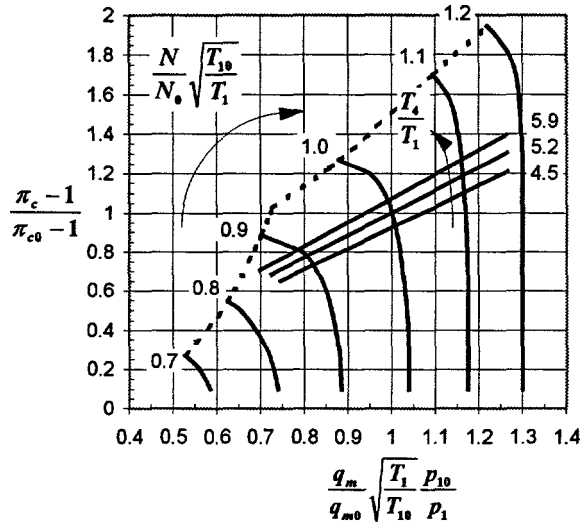

Figure 27. The equilibrium operating diagram for the example case CBE showing the range of possible operating conditions for the compressor.

Table 6. The influence of the individual increase of the parameters p_{amb}, T_{amb}, T_4 and N_{rel} on the terms in the compressor map.

	$\Delta\frac{T_4}{T_1}$	$\Delta\frac{N}{\sqrt{T_1}}$	$\Delta\pi_c$	Δp_2	$\Delta\frac{q_m\sqrt{T_1}}{p_1}$	Δq_m
p_{amb}	0	0	0	+	0	+
T_{amb}	−	−	−	−	±	±
T_4	+	0	+	+	−	−
N_{rel}	0	+	+	+	+	+

Key:

+ increasing	− decreasing
± decreasing in practice	0 no effect

For the case of multi-shaft engines, the determination of the operating point is not so straightforward. For a gas turbine with a detached power turbine for instance, the location of the point is additionally affected by the division of the pressure ratios between the turbines, and by the speed of the gas generator unit. Both of these will be determined to satisfy the power balance for the gas generator and the ellipse law for the low pressure turbine.

To evaluate the magnitude of the influence of using incorrect component characteristics, compressor mass flow map, compressor and turbine efficiency maps, and turbine mass flow characteristics (the ellipse law) have all been considered separately. The erroneousness of modelling mass flows and efficiencies has been characterised by increasing the difference between the corresponding mass flow parameter ($q_m\sqrt{T}/p$), or efficiency, and its design value by 50 % [1]. Table 8 shows the effect of these artificial sources of error for four changes in off-design conditions. The performance values using non-modified characteristics have been presented in Table 7.

Table 7. Performance values for the example cases CBE and CBEX as the basis for Table 8.

	ΔT_4 = -300 K		ΔT_{amb} = -25 K		Δp_{amb} = -10 kPa		ΔN_{rel} = -0.10	
	P_e/P_{e0} [%]	η_e/η_{e0} [%]	P_e/P_{e0} [%]	η_e/η_{e0} [%]	P_e/P_{e0} [%]	η_e/η_{e0} [%]	P_e/P_{e0} [%]	η_e/η_{e0} [%]
CBE	58.8	86.7	122.6	106.4	89.7	99.5	76.8	91.6
CBEX	59.2	79.9	122.9	104.3	89.7	100.5	76.4	101.5

[1] For instance, decreasing the pressure ratio term at a constant speed by 0.2 from its design value in Fig. 5 will cause the mass flow parameter to increase by 0.02. For characterisation, this difference in the mass flow parameter will be increased by 50 % to a value of 0.03.

Table 8. The effect of incorrect component characteristics for the example cases CBE and CBEX. In the model, the difference between the corresponding mass flow parameter ($q_m\sqrt{T}/p$) or efficiency and its design value has been increased by 50 %.

		ΔT_4 = -300 K		ΔT_{amb} = -25 K		Δp_{amb} = -10 kPa		ΔN_{rel} = -0.10	
		$\lvert\Delta P_e/P_e\rvert$ [%]	$\lvert\Delta\eta_e/\eta_e\rvert$ [%]	$\lvert\Delta P_e/P_e\rvert$ [%]	$\lvert\Delta\eta_e/\eta_e\rvert$ [%]	$\lvert\Delta P_e/P_e\rvert$ [%]	$\lvert\Delta\eta_e/\eta_e\rvert$ [%]	$\lvert\Delta P_e/P_e\rvert$ [%]	$\lvert\Delta\eta_e/\eta_e\rvert$ [%]
Incorrect η_{sc}	CBE	0.370	0.281	0.042	0.030	0	0	0.104	0.077
	CBEX	0.371	0.348	0.044	0.040	< 0.001	< 0.001	0.109	0.101
Incorrect q_{mc}	CBE	0.921	0.402	3.643	0.913	0	0	11.507	4.458
	CBEX	0.914	0.068	3.656	0.386	< 0.001	< 0.001	11.699	0.111
Incorrect η_{st}	CBE	1.470	1.470	0.375	0.375	0	0	0.491	0.491
	CBEX	1.510	1.083	0.384	0.241	< 0.001	< 0.001	0.518	0.320
Incorrect q_{mt}	CBE	0.042	0.091	0.004	0.045	0	0	0.128	0.083
	CBEX	0.057	0.030	0.013	< 0.001	< 0.001	< 0.001	0.101	0.004

As the results indicate, incorrect compressor mass flow characteristics are especially prone to introducing considerable inaccuracy in the results if the ambient temperature or speed change. On the contrary, the characteristics of the turbine mass flow have little effect on the results.

The maps used here present changes outside design conditions that may be assumed to have an order of magnitude typical for a variety of gas turbines. Therefore, although the consideration given here is dependent on the component characteristics that have been used, the phenomena can be generalised, to a certain degree, for single shaft gas turbines. Nevertheless, it must be noted that if the maximum efficiency for the components is not attained at the design conditions, as has been the case here, the validity of these results deteriorates. Generally however, the components operate at the design conditions near the maximum efficiency.

6.4.2 Comparison of results

The results of the design calculations are compared to some actual single shaft gas turbines, as given by Larjola et al. [1987]. Table 9 shows values of the main parameters for determining the design performance of these engines, as well as the corresponding net power and efficiency. Due to the fundamental nature of the modelling equations, the accuracy of modelling design performance can, in general, be expected to be high, as will be verified by these results.

Table 9. Comparison of design performance values of some single shaft gas turbines, and the results gained with the model. Ambient conditions are 15 °C and 101.3 kPa, for fuel oil.

	Larjola et al. [1987]						Model	
	T_4 [K]	π_c	q_{ma} [kg/s]	ε	P_e [MW]	η_e	P_e [MW]	η_e
BBC GT9	1271	8.85	163.5	0	34.0	0.269	33.7	0.269
Kongsberg KG2-3R	1083	4.04	13.0	0.80	1.36	0.265	1.36	0.271
Sulzer R7	1198	7.1	66.0	0.76	10.4	0.304	10.5	0.304

To compare the results outside design conditions, Table 10.a shows relative changes in net power and efficiency as a consequence of ambient conditions and speed being individually altered for a modern industrial gas turbine, and the corresponding results using this model. In Table 10.b, the dependency of the net efficiency on the net power is given for the same case. Although no specific component maps were employed to take into account variable compressor geometry for instance, the results agree well with the performance of an actual engine.

Table 10. Performance values of an industrial gas turbine with compressor inlet guide vane control, and the corresponding results gained with this model. No specific component maps were used for the model.

a) The effect of ambient pressure, temperature and speed when alter individually

	Gas turbine		Model	
	P_e/P_{e0}	η_e/η_{e0}	P_e/P_{e0}	η_e/η_{e0}
p_{amb}: 101.3 kPa → 85 kPa	0.840	–	0.832	–
T_{amb}: 15 °C → 40 °C	0.840	0.940	0.812	0.937
N_{rel}: 1 → 0.96	0.958	0.989	0.932	0.985

b) Efficiency and power output

η_e/η_{e0}	P_e/P_{e0}		
	80 %	90 %	110 %
Gas turbine	0.956	0.982	1.015
Model	0.949	0.979	1.015

7 CONCLUSIONS

This study considers the modelling of gas turbine design and off-design performance under steady state conditions, and computing the operating values with a novel approach – by solving the non-linear sets of equations formed by the models. It has specialised in the determination of the performance of industrial scale gas turbines, and the analysis of their behaviour under varying ambient conditions and under different loads. This innovative method has been successfully applied to gas turbine models to provide the performance values, thus replacing common matching techniques that depend on gas turbine configurations.

A gas turbine's performance is dictated by the interaction of its components. Although universal applicability has been of primary interest for determining the operation of these components, constructional characteristics have an influence on the validity of the results outside design conditions. Special attention has been paid to some of these aspects as well. The models presented in this study are especially suitable for industrial scale gas turbines having compressors and turbines typically of the axial and multi-stage type and with a small degree of reaction. For the case of radial components, the accuracy may be expected to be reduced slightly.

In this study, the method used to solve a system of non-linear equations is a modification of Newton's method. The step size is determined so as to decrease the sum of the squares of the functions at the left-hand side of the equation set. This modification converges towards the solution from a wider domain than the basic Newton method. However, no deterministic method can provide convergence from any starting point for a general case and, therefore, as a precondition for this method, a suitable starting point has to be supplied.

For the model in this study, the determination of the starting point for the design state calculation is based on simplifications in the model. For calculations outside design conditions, the result from the design calculus has been applied as the starting point. The same design model is underlying in the off-design model with additional information being supplied to determine the transition from design conditions to off-design. Therefore, the path between the conditions can be divided into sub-intervals and the solution proceeds by applying the result of the previous transition as the starting point for the next one, if necessary.

The suggested method for computing the performance characteristics of gas turbines has proven successful. On comparison with the commonly applied iterative procedures, better control of errors, increased flexibility of modelling, and simplification of the calculation routines has been achieved.

Solving the set of equations, or correspondingly, finding the root of the system, is based on zeroing coordinate functions that are directly derived from the modelling equations. Therefore, controlling the accuracy of the results is easy in the form of the sum of the squares of these functions.

For the selection of the modelling parameters, root finding methods give more freedom since, unlike matching procedures, exchanging these criteria does not itself affect the algorithms. One significant feature of this methodology is the increased freedom for the modelling equations – the implicit relationships between the variables make no difference, only the dependencies of these variables. Therefore, any representation for the component characterising maps, for instance, will be applicable for this model.

The method demonstrated here does not decrease the requirement for knowledge about the theoretical fundamentals underlying these processes, and neither should it since they are the very essence of the mathematical modelling. However, as less attention needs to be paid to the calculation sequences and routines, for instance, the complexity of applying these models is greatly reduced. These models may thus be considered to approach a kind of black box, converting a sufficient amount of input values into output results.

The mathematical models developed in this thesis will provide facilities to optimise the operation of any major gas turbine configuration with respect to the desired process parameters. The computational methods used in this study may also be adapted to any other modelling problems arising in industry.

REFERENCES

Akima, H. (1996). Algorithm 761: Scattered-Data Surface Fitting that Has the Accuracy of a Bicubic Polynomial. *ACM Transactions on Mathematical Software*, Vol. 22, No. 3.

Anderson, J.D. Jr. (1990). Modern Compressible Flow With Historical Perspective, 2nd edition. McGraw-Hill, New-York, USA. ISBN 0-07-001673-9.

Attia, M.S., Schobeiri, M.T. (1995). New Method for the Prediction of Compressor Performance Using One-Dimensional Row-by-Row Analysis. *American Society of Mechanical Engineers Publication 95-GT-434.* New York, USA.

Burden, R.L., Faires, J.D. (1985). Numerical Analysis, 3rd edition. Prindle, Weber & Schmidt, Boston, USA. ISBN 0-87150-857-5.

Cohen, H., Rogers, C.F.C., Saravanamuttoo, H.I.H. (1987). Gas Turbine Theory, 3rd edition. Longman Scientific & Technical, Longman Group Limited, Essex, Great Britain. ISBN 0-582-30539-X.

Dennis, J.E. Jr., Schnabel R.B. (1983) Numerical Methods for Unconstrained Optimization and Nonlinear Equations. Prentice-Hall, Englewood Cliffs, USA. ISBN 0-13-627216-9.

Dixon, S.L. (1984) Fluid Mechanics, Thermodynamics of Turbomachinery, 3rd edition. Pergamon Press, Oxford, Great Britain.

Horlock, J.H. (1985). Axial Flow Turbines. Fluid Mechanics and Thermodynamics, 4th printing. Krieger Publishing Company, Florida, USA. ISBN 0-88275-097-6.

Incropera, F.P., DeWitt, D.P. (1990). Fundamentals of Heat and Mass Transfer, 3rd edition. John Wiley & Sons, Singapore. ISBN 0-471-51729-1.

Ismail, I.H., Bhinder, F.S. (1991). Simulation of Aircraft Gas Turbine Engines. *Journal of Engineering for Gas Turbines and Power.* Vol. 113, No. 1.

Johnson, M.S. (1992). Prediction of Gas Turbine On- and Off-Design Performance When Firing Coal-Derived Syngas. *Journal of Engineering for Gas Turbines and Power.* Vol. 114, No. 2.

Kaikko, J. (1997). Modelling gas turbine design and off-design performance (in Finnish), Master of Science Thesis. Lappeenranta University of Technology, Lappeenranta, Finland.

Kays, W.M., London, A.L. (1984). Compact Heat Exchangers, 3rd edition. McGraw-Hill, New York, USA. ISBN 0-07-033418-8.

Kim, T.S., Kim, J.H., Ro, S.T. (1995). Part Load Performance Enhancement of Gas Turbines by Coolant Flow Rate Modulation. *American Society of Mechanical Engineers Publication 95-CTP-105.* New York, USA.

Kim, T.S., Oh, C.H., Ro, S.T. (1994). Comparative Analysis of the Off Design Performance for Gas Turbine Cogeneration Systems. *Heat Recovery Systems & CHP.* Vol. 14, No. 2.

Korakianitis, T., Wilson, D.G. (1994a). Models for Predicting the Performance of Brayton-Cycle Engines. *Journal of Engineering for Gas Turbines and Power.* Vol. 116, No. 2.

Korakianitis, T., Beier, K.J. (1994b). Investigation of the Part-Load Performance of Two 1.12 MW Regenerative Marine Gas Turbines. *Journal of Engineering for Gas Turbines and Power.* Vol. 116.

Larjola, J. (1982). Transient simulation of gas turbines including the effects of heat capacity of the solid parts. Diss. Helsinki University of Technology, Laboratory of Aerodynamics, Report No. 82-A1, Series A. Otaniemi, Finland.

Larjola, J., Esa, H., Alamäki, J., Paavoseppä, M., Kaikko, J., Isaksson, J., Välimäki, K., Rintamäki, K., Vakkilainen, E. (1987). The development of a domestic gas turbine for energy conversion of medium and low heat value gases (in Finnish), EN B-62. Lappeenranta University of Technology, Lappeenranta, Finland. ISBN 951-763-514-1.

Larjola, J. (1990). Modelling gas turbine design and off-design performance (in Finnish), EN C-49. Lappeenranta University of Technology, Lappeenranta, Finland. ISSN 0785-8248.

Moore, D.F. (1975). Principles and Applications of Tribology. Pergamon Press, Oxford, Great Britain. ISBN 0-08-017902-9

Moran, M.J., Shapiro, H.N. (1993). Fundamentals of Engineering Thermodynamics, 2nd edition. Wiley, New York, USA. ISBN 0-471-59275-7

Morchower, S. (1995). Part Power Modeling of Gas Turbine Engine Systems. *IECEC Paper No. ES-188.* ASME 1995.

Münzberg, H.G., Kurzke, J. (1977). Gasturbinen - Betriebsverhalten und Optimierung. Springer-Verlag, Berlin, Germany. ISBN 3-540-08032-5.

Press, W.H., Flannery, B.P., Teukolsky, S.A., Vetterling, W.T. (1992). Numerical Recipes in FORTRAN: The Art of Scientific Computing, 2nd edition. Cambridge University Press, Cambridge, Great Britain. ISBN 0-521-43064-X.

Reynolds, W.C. (1979). Thermodynamic properties in SI. Department of Mechanical Engineering, Stanford University, Stanford, USA. ISBN 0-917606-05-1.

Schobeiri, T., Abouelkheir, M. (1992). Row-by-Row Off-Design Performance Calculation Method for Turbines. *Journal of Propulsion and Power.* Vol. 8, No. 4.

Seyedan, B., Dhar, P.L., Gaur, R.R., Bindra, G.S. (1995). Computer Simulation of a Combined Cycle Power Plant. *Heat Recovery Systems & CHP.* Vol. 15, No. 7.

Törn, A., Žilinskas, A. (1989). Global Optimization. *Lecture Notes in Computer Science*. Vol. 350. Springer-Verlag, Berlin, Germany. ISBN 3-540-50871-6.

Traupel, W. (1966). Thermische Turbomaschinen, 1. Band, 2. Aufl. Springer-Verlag, Berlin, Germany.

Traupel, W. (1968). Thermische Turbomaschinen, 2. Band, 2. Aufl. Springer-Verlag, Berlin, Germany.

VDI-Wärmeatlas: Berechnungsblätter für den Wärmeübergang (1988), 5. Aufl. VDI-Verlag, Düsseldorf, Germany. ISBN 3-18-400850-9.

Wang, Y. (1991). A New Method of Predicting the Performance of Gas Turbine Engines. *Journal of Engineering for Gas Turbines and Power.* Vol. 113, No. 1.

Watson, L.T., Billups, S.C., Morgan, A.P. (1987). Algorithm 652: HOMPACK: A Suite of Codes for Globally Convergent Homotopy Algorithms. *ACM Transactions on Mathematical Software.* Vol. 13, No. 3.

Wilson, D.G. (1988). The Design of High-Efficiency Turbomachinery and Gas Turbines, 3rd printing. MIT Press, Massachusetts, USA. ISBN 0-262-23114-X.

Zhu, P., Saravanamuttoo, H.I.H. (1992). Simulation of an Advanced Twin-Spool Industrial Gas Turbine. *Journal of Engineering for Gas Turbines and Power.* Vol. 114, No. 2.

LAPPEENRANNAN TEKNILLINEN KORKEAKOULU
LAPPEENRANTA UNIVERSITY OF TECHNOLOGY
TIETEELLISIÄ JULKAISUJA
RESEARCH PAPERS

21. LAATIKAINEN, MARKKU. Stability of aqueous emulsions of synthetic and extracted wood pitches. 1992. 28 s.

22. SUN, ZHENG. Laser beam welding of austenitic-ferritic dissimilar steel joints. 1992. 87 s. Diss.

23. KOIKKALAINEN, PASI. Neurocomputing systems: formal modeling and software implementation. 1992. 142 s. Diss.

24. PIRTTILÄ, TIMO. Empirical analyses of inventory intensity in the Finnish engineering industry. 1992. 118 s. Diss.

25. KOVANEN, M.A. Monte Carlo study of charged particle behaviour in Tokamak plasmas. 1992. U.s. Diss.

26. KALLAS, JUHA et al. Treatment technology of wastewater containing phenols and phenolic compounds. 1992. 40 s.

27. VAKKILAINEN, ESA K. Offdesign operation of kraft recovery boiler. 1992. 83 s. Diss.

28. LAMPINEN, JOUKO. Neural pattern recognition: distortion tolerance by self-organizing maps. 1992. U.s. Diss.

29. PUUMALAINEN, PERTTI. Paperin laadun ja siihen valmistusprosessissa vaikuttavien tekijöiden on-line mittaukset. 1993. 279 s. Väitösk.

30. Second International Seminar of Horizontal Steam Generator Modelling September 29 - 30, 1992, Lappeenranta, Finland. 1993. 195 s.

31. NYKÄNEN, TIMO. M_K-factor equations and crack growth simulations for fatigue or fillet-welded T-joints. 1993. 198 s. Diss.

32. KOSKINEN, JUKKA TAPIO. Use of population balances and particle size distribution analysis to study particulate processes affected by simultaneous mass and heat transfer and nonuniform flow conditions. 1993. U.s. Diss.

33. TUUNANEN, JARI. Thermal-hydraulic studies on the safety of VVER-440 type nuclear power plants. 1994. U.s. Diss.

34. ZHANG, ZHILIANG. A practical micro-mechanical model-based local approach methodology for the analysis of ductile fracture of welded T-joints. 1994. 151 s. Diss.

35. KÄLVIÄINEN, HEIKKI. Randomized Hough Transform: new extensions. 1994. U.s. Diss.

36. HEIKKONEN, JUKKA. Subsymbolic Representations, Self-Organizing Maps, and Object Motion Learning. 1994. 119 s. Diss.

37. KOSKINEN, JUKKA ANTERO. Knapsack sets for cryptography. 1994. 81 s. Diss.

38. TURUNEN, ESKO. A mathematical study of fuzzy logic; an algebraic approach. 1994. U.s. Diss.

39. JANHUNEN, ANTERO. Toimitustäsmällisyyden suunnittelumenetelmä. 1994. 161 s. Väitösk.

40. LARES-MANKKI, LAURA. Strategy implementation bottlenecks: identification, analysis and removal. 1994. 150 s. Diss.

41. French-Finnish Colloquium on Safety of French and Russian Type Nuclear Power Plants. 1994. 275 s.

42. KORPELA, JUKKA. An analytic approach to distribution logistics strategic management. 1994. U.s. Diss.

43. Third International Seminar on Horizontal Steam Generators October 18-20, 1994, Lappeenranta, Finland. 1995. 413 s.

44. AHOLA, JYRKI. Yrityksen strategiaprosessi: näkökohtia strategisen johtamisen kehittämiseksi konserniorganisaatiossa. 1995. 235 s., liitt. Väitösk.

45. RANTANEN, HANNU. The effects of productivity on profitability: a case study at firm level using an activity-based costing approach. 1995. 169 s., liitt. Diss.

46. Optics in Engineering: First Finnish-Japanese meeting Lappeenranta, 12-14th, June 1995 / ed. by P. Silfsten. 1995. 102 s.

47. HAAPALEHTO, TIMO. Validation studies of thermal-hydraulic code for safety analysis of nuclear power plants. 1995. U.s. Diss.

48. KYLÄHEIKO, KALEVI. Coping with technology: a study on economic methodology and strategic management of technology. 1995. 263 s. Diss.

49. HYVÄRINEN, LIISA. Essays on innovativeness and its evaluation in small and medium-sized enterprises. 1995. U.s. Diss.

50. TOIVANEN, PEKKA. New distance transforms for gray-level image compression. 1996. U.s. Diss.

51. EHSANI, NEDA. A study on fractionation and ultrafiltration of proteins with characterized modified and unmodified membranes. 1996. U.s. Diss.

52. SOININEN, RAIMO. Fracture behaviour and assessment of design requirements against fracture in welded steel structures made of cold formed rectangular hollow sections. 1996. 238 s. Diss.

53. OJA, MARJA. Pressure filtration of mineral slurries: modelling and particle shape characterization. 1996. 148 s. Diss.

54. MARTTILA, ESA. Ilmanvaihdon lämmönsiirtimien teknillinen ja taloudellinen mitoitus. 1996. 57 s. Väitösk.

55. TALONPOIKA, TIMO. Dynamic model of small once-through boiler. 1996. 86 s. Diss.

56. BACKMAN, JARI. On the reversed Brayton cycle with high speed machinery. 1996. 103 s. Diss.

57. ILME, JARNO. Estimating plate efficiencies in simulation of industrial scale distillation columns. 1997. U.s. Diss.

58. NUORTILA-JOKINEN, JUTTA. Choice of optimal membrane processes for economical treatment of paper machine clear filtrate. 1997. U.s. Diss.

59. KUHMONEN, MIKA. The effect of operational disturbances on reliability and operation time distribution of NC-machine tools in FMS. 1997. 133 s., liitt. Diss.

60. HALME, JARKKO. Utilization of genetic algorithm in online tuning of fluid power servos. 1997. 91 s. Diss.

61. MIKKOLA, AKI. Studies on fatigue damage in a hydraulically driven boom system using virtual prototype simulations. 1997. 80 s., liitt. Diss.

62. TUUNILA, RITVA. Ultrafine grinding of FGD and phosphogypsum with an attrition bead mill and a jet mill: optimisation and modelling of grinding and mill comparison. 1997. 122 s., liitt. Diss.

63. PIRTTILÄ, ANNELI. Competitor information and competitive knowledge management in a large, industrial organization. 1997. 175 s., liitt. Diss.

64. MEURONEN, VESA. Ash particle erosion on steam boiler convective section. 1997. 149 s. Diss.

65. MALINEN, HEIKKI. Forecasting energy demand and CO_2 -emissions from energy production in the forest industry. 1997. 86 s., liitt. Diss.

66. SALMINEN RISTO T. Role of references in international industrial marketing - a theory-building case study about supplier's processes of utilizing references. 1997. 375 s. Diss.

67. Fourth International Seminar on Horizontal Steam Generators 11-13 March 1997, Lappeenranta, Finland. 1997. 285 s.